AECL-6840

ATOMIC ENERGY OF CANADA LIMITED

L'ENERGIE ATOMIQUE DU CANADA, LIMITEE

# FORMATION, TRANSFORMATION AND DISSOLUTION OF PHASES FORMED ON SURFACES

# CROISSANCE, TRANSFORMATION ET DISSOLUTION DES PHASES FORMEES SUR LES SURFACES

D. W. Shoesmith

Whiteshell Nuclear Research Establishment

Etablissement de recherches nucléaires de Whiteshell

Pinawa, Manitoba R0E 1L0

March 1983 mars

ATOMIC ENERGY OF CANADA LIMITED

# FORMATION, TRANSFORMATION AND DISSOLUTION OF PHASES FORMED ON SURFACES

by

D.W. Shoesmith

Presented as the Lash Miller Award address at the Electrochemical Society Meeting, Ottawa, 1981 November 27.

Whiteshell Nuclear Research Establishment
Pinawa, Manitoba ROE 1LO
1983 March

AECL-6840

# CROISSANCE, TRANSFORMATION ET DISSOLUTION DES PHASES FORMEES SUR LES SURFACES

par

D.W. Shoesmith

## RESUME

On examine dans ce rapport les mécanismes fondamentaux de la croissance des films, de la transformation et de la dissolution des phases formées sur les surfaces. La croissance des films peut se produire par les processus d'état solide ou par la dissolution de la matière en étude (habituellement un métal ou un alliage) et être suivie de la sursaturation et précipitation d'une phase insoluble. La(les) phase(s) formée(s) peut(peuvent) être métastable(s) et se transformer en une(des) phase(s) plus stable(s) soit par les processus d'état solide ou de dissolution-reprécipitation.

Des réactions de dissolution de films peuvent également se produire par une variété de mécanismes, à savoir: (i) la dissolution chimique directe lorsqu'il n'y a pas de changement de l'état d'oxydation; (ii) la dissolution rédox lorsqu'il y a dissolution du film par une réaction rédox mettant en jeu un réducteur ou un oxydant en solution et (iii) l'autoréduction lorsque la dissolution du film est associée à la dissolution du métal.

Ces processus de croissance des films et de dissolution qui produisent souvent des films complexes à plusieurs couches sont courants dans l'industrie nucléaire. On examine un certain nombre d'exemples: (i) la dissolution par oxydation de l'$UO_2$, un mode de libération possible, à partir du combustible irradié, des radionucléides; (ii) la corrosion du fer et de l'acier au carbone dans l'$H_2S$ aqueux qui conduit à la migration du fer et au dépôt des sulfures de fer sur les surfaces et entraîne le bouchage des tubes d'échangeurs de chaleur et des plateaux perforés de colonnes d'échange des usines d'eau lourde employant le procédé Girdler aux sulfures; (iii) la dissolution des films de magnétite à partir des surfaces de fer et d'acier au carbone; la dissolution de ces films est une condition préalable nécessaire pour la décontamination des systèmes de caloporteur primaire des réacteurs CANDU*.

* CANada Deuterium Uranium

L'Énergie Atomique du Canada, Limitée
Établissement de recherches nucléaires de Whiteshell
Pinawa, Manitoba ROE 1LO
1983 mars

AECL-6840

# FORMATION, TRANSFORMATION AND DISSOLUTION OF PHASES FORMED ON SURFACES

by

D.W. Shoesmith

## ABSTRACT

The basic mechanisms of film growth, transformation, and dissolution of phases formed on surfaces are discussed. Film growth can occur via solid-state processes or via substrate (usually metal or alloy) dissolution, followed by local supersaturation and precipitation of an insoluble phase. The phase(s) formed may be metastable and transform to a more stable phase, via either solid-state or dissolution-reprecipitation processes.

Film dissolution reactions can also occur, via a variety of mechanisms including: (i) direct chemical dissolution when no oxidation state change occurs; (ii) redox dissolution when the film dissolves via a redox reaction involving a reducing or oxidizing agent in solution, and (iii) autoreduction, where film dissolution is coupled to metal dissolution.

Such film-growth and dissolution processes, which often produce complex multilayer films, are common in the nuclear industry. A number of examples are discussed: (i) the oxidative dissolution of $UO_2$, a possible mode of release for radionuclides from irradiated fuel; (ii) the corrosion of iron and carbon steel in aqueous $H_2S$, which leads to iron transport and the deposition of iron sulphides on surfaces, causing blockage of heat exchanger tubes and exchange tower sieve trays in heavy-water plants which utilize the Girdler-sulphide process; (iii) dissolution of magnetite films from iron and carbon steel surfaces; dissolution of such films is a prerequisite for the decontamination of CANDU* reactor primary coolant systems.

---

* CANada Deuterium Uranium

Atomic Energy of Canada Limited
Whiteshell Nuclear Research Establishment
Pinawa, Manitoba ROE 1LO
1983 March

AECL-6840

CONTENTS

# 1. INTRODUCTION

The growth of films, and their transformation and dissolution reactions, coupled with such processes as stress and fatigue, are the essence of most industrial corrosion problems. A detailed understanding of the reaction mechanisms is essential if corrosion is to be prevented, or at least controlled. Corrosion studies require a multidisciplinary approach involving chemists, metallurgists and materials scientists. In this review I shall concentrate on the chemical and electrochemical aspects, with particular emphasis on some corrosion processes of interest to the Canadian nuclear industry.

# 2. FILM GROWTH AND DISSOLUTION MECHANISMS

## 2.1 FILM GROWTH

Figure 1 shows, schematically, the variety of possible film growth mechanisms.

Surface films may form via two distinct mechanisms:

(a) The first involves solid state growth, whereby oxidized cationic species (metal ions in the case of oxide growth on metals) are formed and incorporated into the surface film without first dissolving in the liquid. These films grow via the transport of either metal cations from the metal-film interface to the film-solution interface, where they are incorporated into the growing film, or via oxide ion transport in the opposite direction, followed by incorporation into the growing film at the metal-film interface. Under electrochemical conditions, transport occurs under the influence of an electrical potential gradient, and is influenced by the film structure. Factors such as the defect structure and grain size

of the surface film can determine the rate and nature of the film growth process. There have been a number of comprehensive reviews dealing with these factors[1-4] and they will not be discussed in detail here. The film may be composed of more than one phase containing metal cations in more than one oxidation state. These phases may form as distinct layers or, if they form solid solutions, there may be a gradation in stoichiometry through the film.

(b) In systems where the solubility of the cationic species is high, metal dissolution((1) in Figure 1) may accompany the formation of the solid-state base-layer film described above. Metal dissolution is most likely to occur in pores or faults in the base layer, and can produce dissolved material in more than one oxidation state. Dissolving cations can hydrolyze (2) or complex, depending on the pH and composition of the solution, and be transported to the bulk of the solution via diffusion and convection processes (3). If the transport processes are slow compared to the metal dissolution rate, local concentrations of dissolved metal species can supersaturate with respect to metal oxide/ hydroxide phases and precipitation (4) can occur on or near the surface. Precipitation on the surface is most likely since the degree of supersaturation necessary for nucleation will be reduced by the presence of many heterogeneous nucleation sites. In Figure 1 precipitation is shown occurring on top of the base layer. Precipitation in pores or cracks is also possible. The site of precipitation will be determined by a variety of factors, and will be strongly influenced by the relative rates of the dissolution, transport, nucleation and crystal growth processes occurring. The presence of pores and faults, along with processes such as hydrolysis and precipitation, can lead to localized variations in chemical conditions (e.g. changes in pH), and such effects are very important in localized corrosion problems such as pitting and crevice corrosion[5-7].

Supersaturation with respect to more than one phase may occur and consequently a mixed precipitate is often obtained (e.g. $\alpha$-$M(OH)_2$ and $\beta$-$M(OH)_2$ in Figure 1). Which phases form will be determined by the degree

of supersaturation and the relative kinetics of nucleation and crystal growth for the individual phases. Hence it is not uncommon for a metastable phase to form in preference to the stable phase.

Subsequent to precipitation a number of other chemical processes are possible depending on the chemical conditions, or changes thereof. Metastable phases may convert to a more stable phase via either a solid state transformation (5), which may or may not affect the integrity of the crystal, or via a dissolution/reprecipitation process (8). In the latter case, dissolved cationic species (7) may also be transported from the surface into the solution. Finally, an Ostwald ripening (6) of smaller crystals into larger crystals can occur, and again material can be lost from the surface via dissolution and transport to the bulk solution.

The processes of solid-state film growth, precipitation, phase transformation, metal and film dissolution often occur simultaneously. The relative importance of each is determined by the properties of the corroding surface and the environment to which it is exposed.

A common situation is the formation of a dual layer consisting of (i) a porous base layer grown via a solid-state process, and (ii) a precipitated upper layer of individual crystals. A number of examples of such dual-layer growth are listed in Table 1. The nomenclature used in the case of iron sulphides is shown in Table 2. These examples are taken from systems of interest to the nuclear industry and, with the exception of the $Cu/OH^-$ system, will be discussed in more detail in Sections 3.1 to 3.3.

## 2.2 FILM DISSOLUTION PROCESSES

It is obvious from Section 2.1 that substrate and film dissolution are often integral components of the general film growth process. However, in order to dissolve a surface film in an environment different from that in which it is formed, it is necessay to consider the film dissolution process in more detail. Figure 2 shows schematically the

possible mechanisms. For the sake of clarity only a single layer film is shown. A precipitated upper layer would not be expected to react in a fashion drastically different from that of the base layer, although the relative importance of individual reactions may be different. Some of these differences will be discussed in more detail when examples are considered.

There appear to be three distinct mechanisms by which films can dissolve from a surface, as illustrated in Figure 2.

### 2.2.1 Direct Chemical Dissolution

In this case the reaction may be represented by:

$$MO + 2H^{+} \rightarrow M^{2+} + H_2O \qquad (1)$$

The cationic species is transferred from the film matrix to the solution without a change in oxidation state. This process usually involves attack of the oxide by an acidic solution in which the cation has a high solubility. Often the dissolution is assisted by the presence in solution of a strong complexing anion ($A^{-}$) for the cationic species. Prior to removing the cationic species from the surface, the anion may be adsorbed on the surface.

### 2.2.2 Autoreductive Dissolution

Here the cationic species is transferred from the film to the solution in a reduced state, the reducing agent being the underlying substrate. For this mechanism to operate, both the substrate and the film must be exposed to the solution, i.e. the film must be non-continuous. The reaction may be represented by the general scheme:

$$M \rightarrow M^{2+} + 2e \qquad (2)$$

$$M_2O_3 + 2e + 6H^+ \rightarrow 2M^{2+} + 3H_2O \quad (3)$$

2.2.3 Redox Dissolution

In this reaction the film is dissolved by oxidization or reduction of the cationic component to a more soluble oxidation state via a soluble oxidizing or reducing agent in the solution:

$$M_2O_3 + Red + 6H^+ \rightarrow 2M^{2+} + Ox + 3H_2O \quad (4)$$

It is possible for a surface film to dissolve at a rate sufficient to produce supersaturation of a metal salt, especially in acid solutions where the oxide is more soluble than the metal salt. Under these conditions it is possible for the back precipitation of the metal salt to occur. Such reprecipitation processes are often important; for example, such a process is thought to be part of the pitting mechanism[5].

## 2.3 CONTROL OF FILM DISSOLUTION BY EITHER TRANSPORT OR SURFACE REACTIONS

Whether a dissolution reaction is controlled by transport or surface reactions is often of importance in an industrial context. There are several ways to establish which is rate-controlling. If a quantitative knowledge of the contributing reaction steps is required, then the dissolution must be studied under conditions where transport rates are carefully controlled, e.g. at a rotating disk electrode. We have used this method to study the dissolution rate and mechanism for a number of systems including: the dissolution of $PbCl_2$ from Pb surfaces in HCl[8]; the dissolution of $Cu(OH)_2$ from Cu surfaces in concentrated hydroxide[9], and the dissolution of $UO_2^{2+}$ from $UO_2$ surfaces in $Na_2SO_4$ and $Na_2CO_3$[10].

However, it is often impossible to study the desired system in the form of a rotating disk. Consequently, less quantitative methods are required to indicate the nature of the rate-controlling step. A convenient

and simple method is to examine the surface morphology before and after dissolution. If dissolution is fast compared to the rate of transport of dissolved species away from the surface, then the dissolution/deposition process will be close to equilibrium and the overall process will be transport controlled (see Figure 3A). Under these conditions attack of the crystal will be general and no crystallographic etching will be observed.

If transport processes are fast compared to the dissolution reaction, then the surface concentration of dissolved species will be small compared to the equilibrium solubility, and the dissolution process will be surface-reaction controlled. Under these conditions crystal faces may dissolve at different rates and crystallographic etching will be observed (see Figure 3B).

Examples of such microscopic examinations will be shown in Sections 3.1 to 3.3.

## 3. STUDIES OF SPECIFIC SYSTEMS

For the remainder of this review a number of specific film growth/dissolution reactions will be discussed in some detail. An attempt will be made to point out the nature of specific problems encountered in the nuclear industry and to indicate the usefulness of laboratory studies in interpreting and solving, or at least alleviating, the problems. The following topics will be discussed: (i) the oxidative dissolution of $UO_2$, (ii) the corrosion of iron and carbon steel in aqueous $H_2S$, and (iii) the dissolution of magnetite films in solutions containing complexing anions.

### 3.1 OXIDATIVE DISSOLUTION OF $UO_2$

One proposal for disposing of high-level nuclear wastes is to bury them in a vault one kilometre underground in a hard-rock formation

somewhere in the Canadian Shield[11]. To prove the viability of such a proposal it is necessary to study the chemical and physical interactions that might occur in such a repository. Figure 4 shows schematically the waste form (either irradiated $UO_2$ or a glass incorporating radionuclides) and a potential environment. If irradiated fuel is to be disposed of, it is likely that it will be surrounded by a series of barriers including an investment material, possibly Cu or Pb; a metallic container, possibly Ti; and a buffer material, possibly bentonite. The most probable pathway for radionuclide release is by dissolution and transport in groundwater that may contain various chemical species, as indicated on Figure 4. It would be necessary for the groundwater to penetrate the barriers by corrosion processes in order to attack the fuel or glass. For radionuclides to totally escape from the waste vault they would also have to penetrate these barriers, and then avoid entrapment by the other potentially reactive environments they would encounter.

Figure 5 shows schematically the expected fate of radionuclides released from the waste form, shown at the left of the figure. Release of actinides and fission products could occur via two distinct mechanisms:

(a) Leaching, whereby the radionuclide is released but the waste form matrix remains intact.

(b) Matrix dissolution, whereby the waste form dissolves and in so doing releases the radionuclides.

The bottom part of Figure 5 indicates reactions that could occur in the groundwater. These include hydrolysis (depending on the species and the pH), polymerization, colloid formation and/or precipitation. Alternatively, complexation (possibly with carbonate) could lead to dissolved-ion transport.

Across the top of the figure the surfaces to which the radionuclide will be exposed are shown, and the nature of possible surface

reactions is indicated. The dashed arrows indicate that subsequent to reaction with a surface, the radionuclide may not be irreversibly trapped but could be re-released to the groundwater.

The possibilities for film growth/dissolution reactions are numerous, but this review will concentrate on the first in the sequence, the release mechanisms from uranium dioxide fuel. The determination of the $UO_2$ dissolution mechanism under oxidizing conditions will be described. Radionuclide release appears to be an extremely complicated process[12], and the work described here should be considered as a fundamental base upon which to study the more applied aspects of the problem[13].

Thermodynamic calculations and experimental measurements show that the solubility of $UO_2$ is very low under reducing conditions[14-16]. However, in the presence of oxidizing agents the solubility is substantially increased due to the formation of U(VI) species. Consequently, the most favourable conditions for fuel dissolution would be oxidizing conditions. Hence, a knowledge of the behaviour of $UO_2$ under various redox conditions is essential to determine the conditions under which it is stable and those under which it will dissolve.

Electrochemical methods are the most powerful for studying surface reactions under controlled redox conditions, and consequently the oxidative dissolution of $UO_2$ has been studied using a variety of them[10,13].

Figure 6 shows a series of potentiostatic oxidations of $UO_2$ at different applied potentials in 0.5 mol·dm$^{-3}$ $Na_2SO_4$ at pH = 3.8. At potentials ≈ +100 mV (vs. the saturated calomel electrode, SCE) the log current versus log time is linear, indicating solid-state film growth[4]. At higher anodic potentials, the deviation from linearity at long times indicates a parallel dissolution reaction. The dissolution product has been shown to be $UO_2^{2+}$ [17], in this case complexed by the $SO_4^{2-}$ ion to give $UO_2SO_4$. The higher the anodic potential the greater the deviation from

linearity, and hence, the larger the dissolution contribution. For potentials $\gtrsim$ +350 mV, the dissolution reaction is totally dominant, as indicated by the current being almost time-independent. One might conclude that the reaction is simply formation of a film in an intermediate oxidation state followed by its oxidative dissolution, i.e.

$$UO_2 \rightarrow (U^{V}\text{film}) + e \tag{5}$$

$$(U^{V}\text{film}) \rightarrow UO_2^{2+} + e \tag{6}$$

$$UO_2^{2+} + SO_4^{2-} \rightleftharpoons UO_2SO_4 \tag{7}$$

This mechanism has been proposed[17,18] and indeed may be a reasonable representation of the behaviour in acid solutions.

However, in a waste vault, $UO_2$ is more likely to be exposed to solutions in the neutral pH range (5 to 10), and experiments at such pH values show a more complicated behaviour for $UO_2$ oxidation. Figure 7 shows a series of cyclic voltammograms to various anodic potential limits at pH = 10.5, recorded at a sweep rate of 20 $mV \cdot s^{-1}$. The voltammograms show a number of stages of oxidation prior to the large increase in anodic current for potentials > 0.000 volts. For positive potentials the current is being used predominantly in the production of dissolved $UO_2^{2+}$. At the lower potentials, two stages of surface oxidation, marked (a) and (b) in Figure 7, are observed. These films can be stripped off on the cathodic cycle at the peaks marked (a) and (b), respectively. The shoulder on the anodic sweep, marked (c), does not lead to a separate reduction peak and appears to be an artefact caused by surface roughness[10]. If the anodic sweep is allowed to extend to +0.500 volts where the current is large and dissolution, as $UO_2^{2+}$, is extensive, then a third reduction peak, marked (d) in the figure, is observed. If the disc-shaped electrode is rotated, peak (d) is not observed, indicating that it is due to the reduction of a film formed by dissolution, local supersaturation, and back precipitation onto the electrode. When the electrode is rotated, the dissolved $UO_2^{2+}$ is

transported from the electrode surface, and local supersaturation and precipitation do not occur.

Figure 8 shows the forward anodic sweep of Figure 7, and also shows the steady-state currents observed if the potential is held constant and the current recorded after it has decayed to a constant value. For potentials < +0.100 volts, the potentiostatic current falls to extremely small and generally slightly negative values. For values > +100 mV, the steady-state current is positive and can be shown to be due to dissolution by comparing the charges measured by current integration to the analyzed amount of uranium in solution. Consequently, we can separate the oxidative behaviour of $UO_2$ into two regions: (i) for $E \leq +100$ mV, the current is transitory and results in surface film growth with minor amounts of dissolution; (ii) for $E \geq +100$ mV, the current over an extended period of time is due to dissolution as $UO_2^{2+}$. However, even at these higher potentials the initial current goes to film formation, as indicated by the charge measurements shown in Figure 9. The anodic charges ($Q_A$) were obtained by integration of potentiostatic current-time transients, and the cathodic charges ($Q_C$) by integration of cathodic voltammetric sweeps similar to the reverse sweeps shown in Figure 7. The cathodic charges are a measure of the film thickness. For the first 100 seconds of oxidation the anodic and cathodic charges are approximately equal, indicating that all the anodic charge is going to produce a surface film.* For times greater than $\sim$ 1000 seconds the film charge is constant, whereas the anodic charge continues to increase linearly. Under these conditions the charge is all going to dissolution, the film thickness remaining constant.

The nature of the films formed on $UO_2$ under electrochemically oxidizing conditions has been determined by X-ray photoelectron spectroscopy (XPS). The films were grown potentiostatically for a given length of time and then analyzed by XPS. The details of these measurements have been

* The small discrepancy between anodic and cathodic charges is probably due to an inability to separate the current due to film reduction from the current due to $H_2$ evolution, the film reduction possessing a tail obscured by $H_2$ evolution.

discussed elsewhere[19]. For present purposes it is sufficient to say that XPS yields a measure of the ratio of $U^{VI}$ to $U^{IV}$ in the surface film. Figure 10 shows the ratio plotted as a function of oxidation time for potentiostatic oxidation at +300 mV at pH = 7. The behaviour is similar at other pH values in the range 6 to 10. The dotted lines and arrow indicate the ratios expected for films of composition $U_4O_9$, $U_3O_7$, $U_2O_5$ and $U_3O_8$, respectively. One can see that the oxidation does proceed through a series of stages, with $U_3O_7$, $U_2O_5$ and $U_3O_8$ occurring on the surface at different times.

On the basis of electrochemical and XPS measurements of this kind one can write the following scheme for oxidation and dissolution of $UO_2$:

OXIDATIVE DISSOLUTION OF $UO_2$

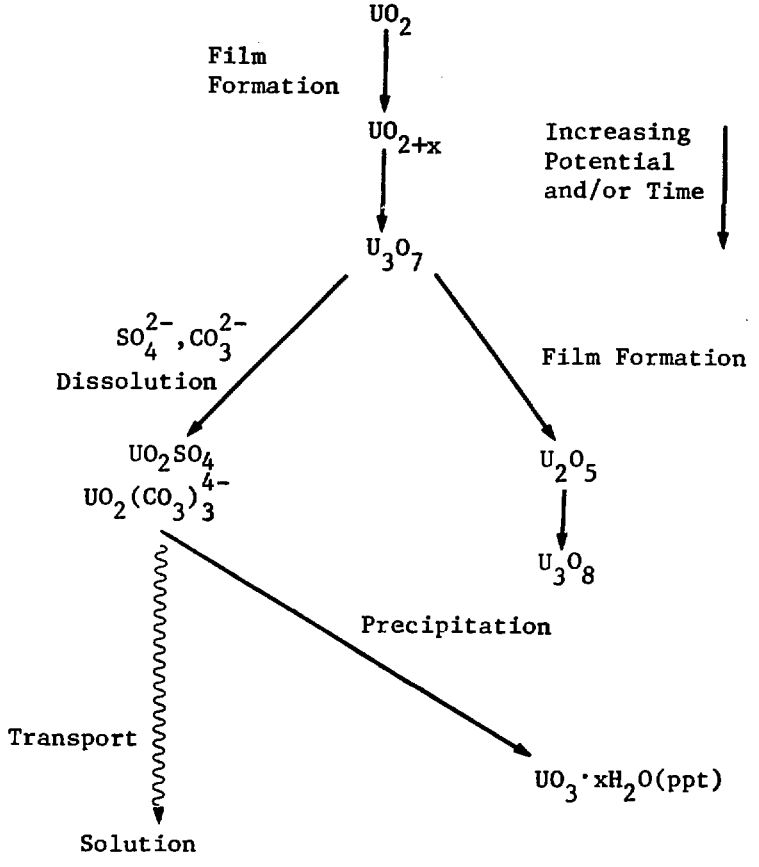

The first two stages of film growth ($UO_{2+x}$, $U_3O_7$) are fast compared to the subsequent stages ($U_2O_5$, $U_3O_8$), and occur prior to the onset of dissolution. Dissolution appears to start once $U_3O_7$ is formed and is accelerated by $CO_3^{2-}$. This behaviour can be rationalized in terms of the oxide structures. Up to and including the formation of $U_3O_7$, no major structural rearrangement of the basic $UO_2$ lattice is required. Oxidation can be envisaged as occurring by $O^{2-}$ takeup at interstitial sites in the $UO_2$. Dissolution commences when a major structural rearrangement is required for further oxide growth, i.e. for $U_2O_5$ and $U_3O_8$ growth. These last stages of film growth are slow (Figure 10) and film growth and dissolution can be envisaged as occurring through a common intermediate:

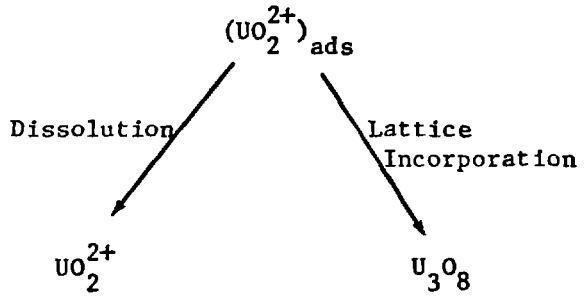


(9)

The surface coverage by $(UO_2^{2+})_{ads}$, and therefore the composition of the surface oxide, will be determined by the potential.

It is obvious from the above reaction scheme that a small degree of surface oxidation can be tolerated without significant dissolution occurring, and an arbitrary potential barrier can be drawn to separate this region from the region where oxidation will lead to dissolution. This is indicated by the vertical shaded area in Figure 8. Consequently, on the basis of the above experiments, it is possible to define the redox conditions under which $UO_2$ is stable or unstable.

Figure 11 shows two photomicrographs of the $UO_2$ electrode surface. Figure 11A shows the surface prior to dissolution, and Figure 11B

shows the surface after 78 days of constant current dissolution (10 μA) in 0.5 $mol \cdot dm^{-3}$ $Na_2SO_4$ + 0.01 $mol \cdot dm^{-3}$ $Na_2CO_3$ (pH = 10.3). Under these conditions the dissolution is surface-reaction controlled, as indicated by the crystallographic etching of the $UO_2$ particles. The pits are caused by particle erosion from the $UO_2$ surface. If dissolution were continued for longer times it is obvious that the pressed sintered pellet could break up, thereby maximizing the surface area available for dissolution. Under these accelerated dissolution conditions it is clear that the sites most susceptible to dissolution are the grain and particle boundaries. This behaviour could have a major impact on the rate of radionuclide release, since certain radionuclides gather at grain boundaries and would therefore be more quickly released if dissolution occurred preferentially at these sites[20]. Whether this kind of behaviour will be observed under conditions less aggressive than those used in the above experiments remains to be determined.

## 3.2 CORROSION OF IRON AND CARBON STEEL IN AQUEOUS $H_2S$

The corrosion of carbon-steel surfaces leads to a number of problems in heavy-water production plants that use the Girdler-sulphide process. This process employs the temperature-sensitive reversible reaction

$$H_2O(l) + HDS(g) \rightleftharpoons HDO(l) + H_2S(g) \qquad (10)$$

to extract deuterium occurring naturally in water. At the high temperature employed, the gas phase is enriched in deuterium compared to the situation at low temperature, and practical use is made of this effect by contacting a countercurrent flow of water with $H_2S$ in large sieve-tray towers. By using three such towers, arranged consecutively, about 20% of the deuterium is extracted from the feedwater, which has an initial deuterium content of ≈ 150 μg/g*[21,22]. Figure 12 shows the tower arrangement. The water

* The deuterium isotopic content of the Lake Huron feedwater for the Bruce Heavy Water Plant.

cascades down the tower across a series of sieve trays and $H_2S$ flows up the tower through holes in the trays to ensure efficient mixing (see inset, Figure 12). A common problem is the corrosion of the carbon-steel surfaces in the cold section of the tower where the pressurized aqueous $H_2S$ environment ($p_{H_2S} \simeq 2$ MPa) causes the release of soluble ferrous ion. When the dissolved iron contacts hotter surfaces in the bottom portion of the tower it tends to deposit, mainly on the stainless-steel sieve trays and on the hot (up to 160°C) stainless-steel surfaces of the heat exchangers (shaded areas in Figure 12). There are a number of consequences, the most significant being the blockage of sieve-tray holes leading to a loss of mixing efficiency, and the loss of heat transfer efficiency in the exchangers.

The movement of soluble iron from corroding carbon-steel surfaces to non-corroding* stainless-steel surfaces is often referred to as iron transport[23], and Figure 13 shows this schematically. To understand, and hence solve this problem, it is necessary to answer a number of questions:

(a) What is the nature of the corrosion layer?

(b) How is it formed and what is the impact of factors that vary within the plant (i.e. pressure of $H_2S$, temperature, fluid flow conditions)?

(c) What is the rate of iron dissolution from the carbon steel?

(d) How does this dissolution rate vary with the nature of the corrosion film?

(e) Why do sulphides deposit on stainless steel?

* In this context "non-corroding" should not be taken to mean that no corrosion occurs, but only that the stainless steel is not a major source of soluble iron.

(f) What is the nature of the deposited film on stainless steel?

A discussion of all these aspects is beyond the scope of this review. Discussion will be concentrated on aspects of the corrosion mechanism, since the proposed solution to the iron transport problem involves a conditioning of the carbon-steel surfaces, based on an understanding of the corrosion mechanism[24].

Examination of corroded samples from various surfaces in a heavy-water plant indicated a very complicated corrosion mechanism, and this was borne out by a variety of laboratory and engineering loop experiments. The corrosion scheme based on these studies[25-37] is shown below. Table 2 lists the iron sulphides and indicates their composition.

The first stage in the corrosion of carbon steel in aqueous $H_2S$ is the formation of a mackinawite ($FeS_{1-x}$) layer, via a solid-state mechanism (see corrosion sequence (11)). This layer grows very quickly. For instance, at 25°C in water saturated with $H_2S$ gas, a black film of mackinawite is visible on iron or carbon steel after only a few seconds. This film rapidly thickens, developing substantial stresses in the process. When these stresses are relieved by cracking, erosion and the development of a more porous layer[27], high rates of local iron dissolution occur, leading, under relatively static conditions, to local supersaturation with respect to a number of other phases. Consequently, a second precipitated layer of mackinawite, cubic ferrous sulphide $(FeS)_c$ and troilite $(FeS)_t$ is formed. Cubic ferrous sulphide is metastable with respect to mackinawite and is transformed via a solid-state mechanism. The stages of corrosion beyond troilite are more difficult to achieve, as will be discussed.

When further reaction occurs, troilite appears to convert to pyrrhotite ($FeS_{1+x}$) via both a solid-state mechanism and a dissolution/reprecipitation mechanism[29,30]. The conversion of pyrrhotite to pyrite ($FeS_2$), and sometimes marcasite ($FeS_2$), involves further oxidation (from $S^{2-}$ in FeS to $S^-$ in $FeS_2$) and occurs by dissolution followed by an

CORROSION SEQUENCE FOR IRON/CARBON STEEL IN AQUEOUS $H_2S$ (11)

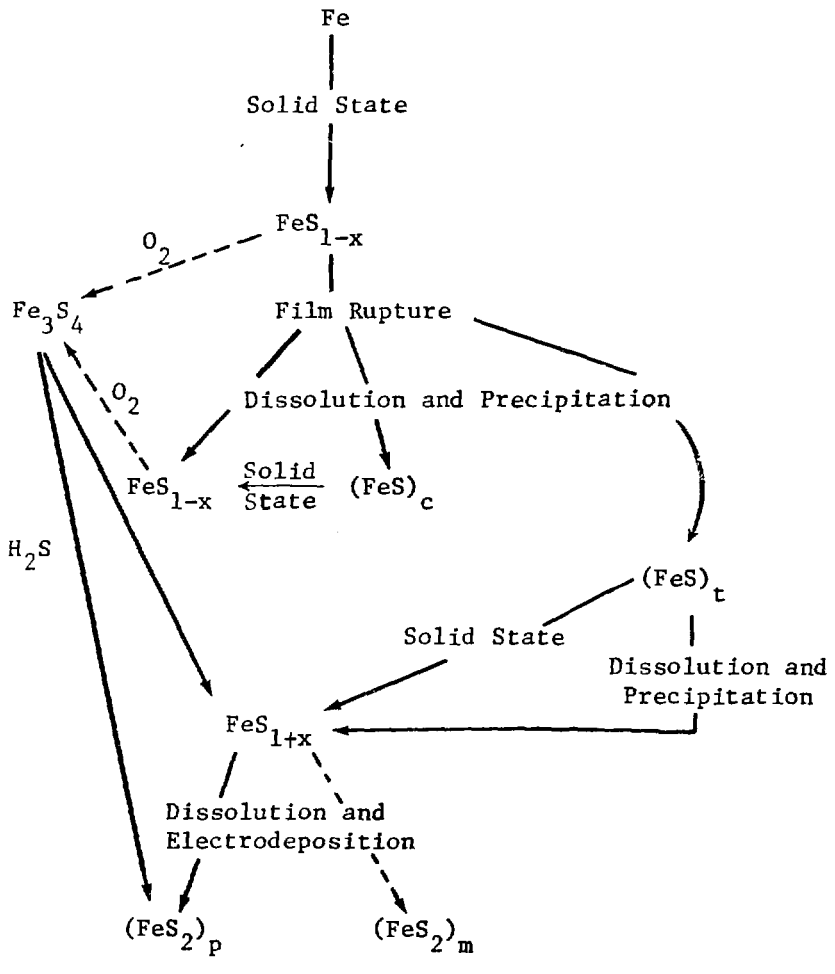


| $Fe^{2+}$ release rate for stage opposite | $mol \cdot m^{-2} \cdot s^{-1}$ at 298 K and pH = 3.5 |
|---|---|
| | $\approx 2 \times 10^{-6}$ |
| | $\geqslant 2 \times 10^{-6}$ |
| | $8 \times 10^{-7}$ |
| | $(1 \text{ to } 5) \times 10^{-9}$ |
| | $8 \times 10^{-11}$ |

——→ Main Corrosion Sequence

- - - - → Effect of External Oxidants

electrocrystallization (or electrodeposition) step. The dashed lines shown in corrosion sequence (11) indicate the consequence of introducing $O_2$ into the corrosion environment.

The advantage of obtaining a surface covered by pyrite is obvious from the $Fe^{2+}$ release rates shown on the right hand side of the corrosion sequence schematic. These values are based on measurements of the solubilities and dissolution rates of the various phases[25], and indicate a decrease in release rate of 4 to 5 orders of magnitude between mackinawite and pyrite.

Figure 14 shows the distribution of phases observed when iron (or carbon steel) is corroded in $H_2S$-saturated water at 21°C. X-ray peak heights have been used to estimate the amount of each phase present on the surface. Obviously, the data are only semi-quantitative. As stated above, the initial layer of mackinawite forms very quickly, and scanning electron microscopy (SEM) shows that this film cracks and spalls from the electrode during the first hour or so of corrosion (see Figure 15). Once this film breaks down, cubic ferrous sulphide forms and becomes the predominant surface phase during the first 50 hours or so of corrosion. Troilite, the stable phase under these conditions, grows in only slowly over this time period (Figure 14 and Figure 15). According to the data of Figure 14, the amount of mackinawite remains constant during this time period. This is not the case, however, as mackinawite is forming continuously but spalls from the surface and collects as a loose deposit in the reaction vessel.

For $50 < t < 100$ hours the amount of the more stable phase, troilite, continues to increase steadily, but the amount of cubic ferrous sulphide falls dramatically, accompanied by a corresponding increase in the amount of mackinawite on the surface. This is due to the solid-state transformation of the cubic ferrous sulphide to the more stable mackinawite. This transformation has been followed in detail by X-ray diffraction (XRD) in a separate experiment in dry air and the results are shown in Figure 16. The conversion is quantitative during the first 40 to

60 hours and fits an Avrami relationship for the instantaneous nucleation of mackinawite centres[27]. At longer times there is a discrepancy between the amount of cubic ferrous sulphide disappearing and mackinawite being formed. This is because the X-ray experiment was carried out in dry air, and small amounts of mackinawite are converted to greigite ($Fe_3S_4$) by reaction with $O_2$.

Information on the relative kinetics of formation of the individual phases can be obtained from electrochemical experiments. If a constant current is applied to the corroding electrode, then the corrosion reaction can be inhibited or accelerated depending on whether the current is cathodic or anodic, respectively. The relative amounts of each phase on the surface (from XRD) are shown as a function of the applied current in Figure 17. In the bottom half of this figure an attempt is made to show schematically observations from SEM experiments. If a large cathodic current is applied, the corrosion current is reduced to a small value and a coherent layer of mackinawite is formed which thickens only slowly; hence little stress builds up and cracking does not occur so readily. Around zero applied current (the natural corrosion condition) the initially formed mackinawite base layer cracks and an upper layer of cubic ferrous sulphide and troilite is formed, as discussed above. As the applied current is increased, the amount of troilite formed increases and the amount of cubic ferrous sulphide decreases. This behaviour indicates that there is a competition for soluble material between these two phases and that troilite requires a higher local supersaturation (achieved at the higher applied currents). This suggests that the slow step for troilite formation is nucleation. Supporting evidence for this contention was obtained by using a temperature pulse under natural corrosion conditions, which showed that troilite, nucleated readily at 70°C, continued to grow (as opposed to cubic ferrous sulphide) when the temperature was reduced to 25°C. When a large anodic current is applied, the amount of both precipitated phases decreases and the amount of mackinawite increases. Under these conditions a steady erosion of mackinawite occurs. When film cracking occurs, the film repair process is too fast to allow significant metal dissolution and consequently little precipitated material is obtained. The observed behaviour can be

represented by the following reaction scheme, where the sulphide nomenclature is defined in Table 2.

REACTION SCHEME FOR THE EARLY STAGES OF IRON CORROSION IN AQUEOUS $H_2S$ (12)

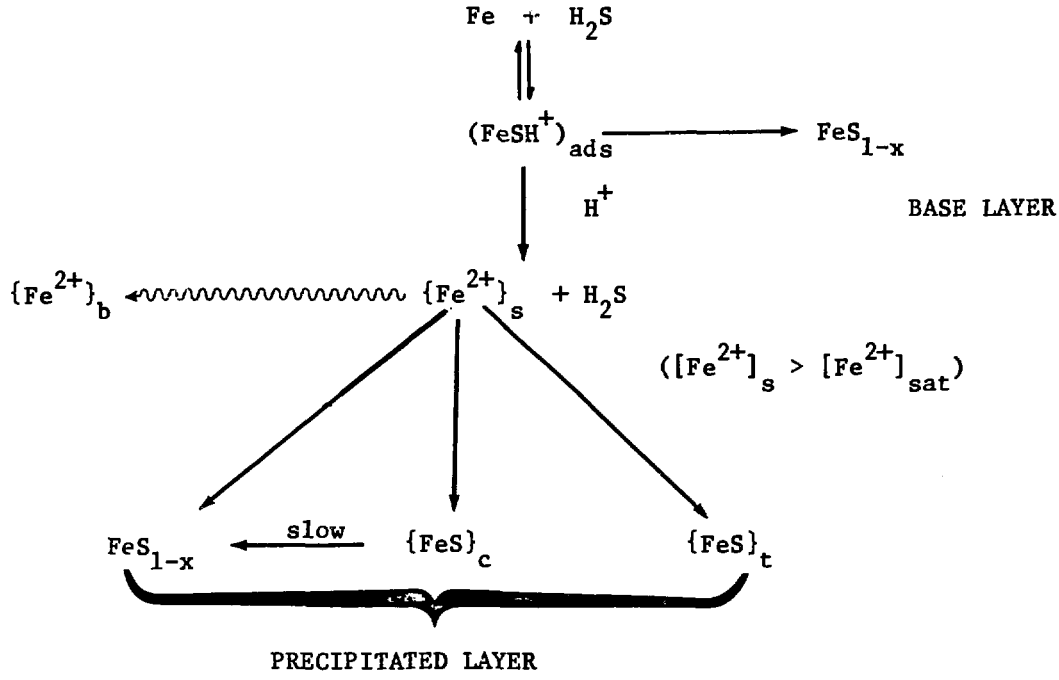


($\{Fe^{2+}\}_s$ in solution near corroding surface, $\{Fe^{2+}\}_b$ in the bulk solution)

Some details of this scheme are discussed more fully in reference 27. With stirring it is possible to reduce the local surface concentration of dissolved iron below the saturation value with respect to the precipitated phases and thereby prevent their formation. When this occurs the solid-state grown mackinawite film is the only film formed. Not only does this film allow a high $Fe^{2+}$ dissolution rate[32,35] but it continually erodes, offering very little protection against continued corrosion. This situation has been observed in heavy-water plants, especially at pipe bends where the solution is flowing very quickly, and a number of pipe failures have been attributed to this kind of erosion process.

The stages of corrosion beyond troilite are much slower than the initial stages discussed above and are very slow at low temperatures. Figure 18 summarizes the effect of several variables on the conversion: troilite → pyrrhotite → pyrite. These effects will only be discussed superficially here (see references 25-37 for detailed discussion).

Temperature variation has a major impact on the rate of formation of pyrrhotite and pyrite, which explains why the carbon-steel walls of the hot tower (135°C) are covered with these two phases and hence do not undergo corrosion to the same extent as those in the cold tower.

Stirring strongly influences the later stages of the corrosion reaction with the major influence in the final stage - the conversion of pyrrhotite to pyrite. This reaction proceeds via a dissolution-electrocrystallization (deposition) step. The dissolution and deposition sites are illustrated in the scanning electron micrograph of Figure 19, which shows the surface of a troilite crystal after six days' exposure to aqueous $H_2S$ at 130°C. This crystal surface was in partial contact with the vessel wall so that a small volume of stagnant solution was trapped between the wall and the crystal surface. This ensured that, when troilite dissolution occurred, the dissolved $Fe^{2+}$ was not transported away from the surface. Since supersaturation with respect to pyrite formation is possible under these conditions, pyrite nucleation and growth is observed. However, supersaturation alone is an insufficient condition for pyrite formation; oxidation of sulphide to polysulphide is also necessary, i.e.

$$2S^{2-} \rightarrow S_2^{2-} + 2e \qquad (13)$$

Electrochemical experiments at stainless-steel surfaces[33] indicate that the crystallization of pyrite is an electrochemical reaction. In the experiment described above the troilite/pyrrhotite surface could act as an electronically conducting surface capable of separating anodic and cathodic sites. The corresponding cathodic reaction would be reduction of protons to hydrogen, and hydrogen formation has been observed in autoclave

experiments where pyrite formation is copious[36]. The layered etchpit formation observed in Figure 19 parallels the layered crystal structure of troilite/pyrrhotite, and indicates that the dissolution reaction is the rate-controlling step in the overall process (see Section 2.3).

The last factor, (d), in Figure 18 is the presence of an anodic sink in the form of a stainless-steel surface. When carbon steel was corroded in the presence of a stainless-steel surface, pyrite tended to crystallize on the stainless-steel surface but not on the carbon steel. This behaviour is very similar to that observed in heavy-water plants. Figure 20 shows the potentials measured on a carbon steel and a stainless-steel electrode exposed to aqueous $H_2S$ in the same autoclave. The potential of the stainless steel is > 100 mV more anodic than that of the carbon steel, making stainless steel a more favourable surface for the oxidation of sulphide to polysulphide, a necessary condition for pyrite formation.

If a passivating pyrite layer is desired on carbon steel to minimize iron dissolution then, from the data of Figures 18 to 20, we would suggest carbon steel be preconditioned under the following conditions:

(i) high temperature
(ii) high $H_2S$ pressure
(iii) stagnant solution
(iv) no anodic sinks

Such a method has indeed been proposed for preconditioning heavy-water plants[23] and appears to be successful.

## 3.3 DISSOLUTION OF MAGNETITE FILMS FROM IRON AND CARBON-STEEL SURFACES

In the above two sections the situations discussed involved predominantly film growth processes. In this section the main process is oxide dissolution.

During normal operation of a CANDU reactor (and other water-cooled reactors) corrosion of construction materials occurs. In CANDU systems this is predominantly carbon-steel corrosion. Despite careful control of chemical conditions, corrosion does occur and small amounts of metallic ions enter the coolant circuit. Eventually, this leads to the circulation of both dissolved and particulate species through the reactor core. These species are deposited on the fuel and become activated, producing radioactive metallic species which are re-released to the coolant and recirculated, as dissolved ions or particles, to the out-core boiler circuits, where they become incorporated in the corrosion films growing on the boiler circuit surfaces. This process is shown schematically in Figure 21. A number of radioactive metallic species are formed, the most important of which is $^{60}Co$, with a half-life of 5.65 years.

Extensive studies of this process, known as activity transport, have produced a good mechanistic understanding[38-40]. The film formed possesses the common dual-layer structure discussed above. In this case, however, a third particulate layer is formed, by deposition of particulate material circulating in solution.

Activity transport leads to a steady buildup of radiation fields around the reactor and eventually the radioactive material must be removed. This process is known as decontamination and a successful method, CAN-DECON, has been developed[41].

The main requisite of a decontamination process is that it remove the radioactivity without harming the integrity of the construction materials. The most effective means of removing radioactivity is to dissolve the oxide film in which it is incorporated. However, this could introduce a number of adverse effects. If the reagent is too aggressive, the underlying metal or alloy could be corroded. Also, once the protective oxide film has been removed, corrosion of the metal or alloy will be accelerated when the reactor is returned to normal operation, possibly

leading to a fast reactivation. The CAN-DECON process successfully avoids most of these pitfalls. Some of the practical aspects of decontamination have been discussed elsewhere[41,42].

Given the importance of achieving a successful reactor decontamination, a fundamental knowledge of the mechanism and kinetics of oxide-dissolution processes and how they are affected by reagents, added for a variety of reasons, is essential. The oxide films observed on boiler circuit walls are predominantly magnetite and the predominant surface is carbon steel. Any efficient oxide dissolving solution is likely to contain reagents such as:

(a) complexing agents to increase solubility,

(b) redox reagents to adjust the oxidation state of the metal ions in the oxide film to their most soluble oxidation state, and

(c) corrosion inhibitors to prevent corrosion of the exposed metal.

The remainder of this review will consider the mechanism of magnetite dissolution from iron surfaces and how it is affected by various reagents. Some general principles that should apply to the dissolution of other oxides from surfaces other than iron and carbon steel* will be discussed.

Films were grown in 1.0 mol·dm$^{-3}$ NaOH solutions at 280°C under reducing conditions, i.e. a slight overpressure of hydrogen. A typical film (Figure 22A), is composed of a base layer of magnetite covered by an upper layer of hexagonal magnetite crystals. The films were formed on iron or carbon-steel coupon-like electrodes which were then exposed to a

* The mechanism of dissolution of magnetite is essentially the same from both iron and carbon-steel surfaces.

solution in which we wished to follow the dissolution reaction. The corrosion potential of the electrode was monitored against a saturated calomel electrode and the solution was sampled at regular intervals and analyzed for dissolved iron. The experimental setup is given elsewhere[43].

Figure 23 shows the corrosion potential and amount of dissolved iron for magnetite-covered iron discs in 2 x $10^{-3}$ mol•$dm^{-3}$

sodium ethylene-diaminetetracetate (pH = 3.3; T = 21°C) as a function of time. The dissolution behaviour can be separated into three distinct regions:

(a) In region I the potential is > -100 mV and the amount of iron dissolved is undetectable.

(b) In region II the potential falls to a second plateau and the iron release rate accelerates.

(c) In region III, which starts after 1.5 hours, the potential falls rapidly to < -500 mV and the rate of iron release decreases.

The efficiency of the dissolution reaction is very low. After 7 hours only ≈ 13% of the film has been dissolved and even after 24 hours ≈ 50 to 60% of the film remains on the surface. Obviously, this solution, under these conditions, is not too useful for magnetite dissolution.

Figure 24 attempts to show schematically the mechanism of dissolution and the reasons why oxide dissolution is so slow and inefficient. In region I of Figure 23, only the oxide is exposed to solution and the only possible mechanism for oxide dissolution is direct chemical dissolution, as $Fe^{2+}$ and $Fe^{3+}$. This process is obviously extremely slow under the conditions used since no dissolved iron is detectable.

In region II, oxide dissolution is via an autoreductive process (see Figure 24) with metal dissolution occurring from the metal surface exposed at the base of pores in the base layer. In this region, oxide dissolution is probably occurring with reasonable efficiency.

In region III, the major potential transition from region II leads to an electrode potential at which proton reduction is also possible. Hence, there is a competition for electrons (released by metal dissolution) between the reduction of protons to hydrogen gas and the reduction of ferric ion to the more soluble ferrous ion. Obviously, the kinetics favour proton reduction, and reductive dissolution of the oxide proceeds very slowly.

The situation in region III is potentially dangerous. Most of the surface is oxide-covered and corrosion can continue at the base of the pores, which could lead to substantial pitting. The scanning electron photomicrograph in Figure 22C shows the surface after 7 hours of dissolution. The upper-layer crystals are only slightly attacked. The base layer can be seen to be full of a large number of small pores. These pores were probably present during film growth at high temperature[44,45], the upper layer growing as a consequence of metal dissolution at the base of these pores. In fact, it can be demonstrated that the degree of porosity of this base layer is all-important in determining the dissolution behaviour of such films[43].

Obviously, dilute, slightly acidic EDTA solutions at room temperature are not particularly useful for removing magnetite films from iron or carbon steel surfaces, and a number of obvious remedies do not work particularly well. For instance, an increase in EDTA concentration tends to accelerate metal dissolution but not oxide dissolution. An increase in pH will accelerate oxide dissolution, but accelerates metal dissolution even more. The best remedy is an increase in temperature to above 70°C, whereby all the oxide can be removed.

If magnetite reduction ($Fe^{3+}$ to $Fe^{2+}$) is a prerequisite for oxide dissolution, then the addition of a reducing agent should accelerate the process, and perhaps also avoid possible corrosion problems associated with the autoreductive mechanism described above. One potential reducing agent is oxalic acid, which has the advantage that its decomposition products ($CO_2$ and $H_2$) should not be harmful when the decontaminated reactor is restarted. The overall reductive dissolution process can be represented by the equation

$$Fe_3O_4 + H_2C_2O_4 + 6H^+ \rightarrow 2CO_2 + 4H_2O + 3Fe^{2+} \qquad (14)$$

The addition of even small amounts of oxalic acid to the solution previously used has a major impact on the amount of oxide dissolved, as shown in Figure 25. At a concentration as low as $5 \times 10^{-5}$ $mol \cdot dm^{-3}$ the fraction of oxide removed increases to $> 0.6$ compared to $< 0.2$ in the absence of oxalate. The experiments lasted six hours, and the fraction removed was estimated from XRD data[46].

The iron dissolves in both the $Fe^{3+}$ and $Fe^{2+}$ states (see Figure 26) indicating that, for concentrated oxalate solutions ($\gtrsim 10^{-2}$ $mol \cdot dm^{-3}$), direct chemical dissolution predominates over reductive dissolution. The ferric ion is complexed by the oxalate anion in solution:

$$Fe_3O_4 + 2H_2C_2O_4 + 4H^+ \rightarrow 2FeC_2O_4^+ + Fe^{2+} + 4H_2O \qquad (15)$$

The plateau in the $Fe^{3+}$ curve coincides with the complete removal of the oxide film. For times $> 2$ hours, the released ferrous ion arises from metal dissolution, the very slow release rate being due to the inhibition of ferrous ion release by precipitation of a layer of β-ferrous oxalate dihydrate on the metal surface:

$$Fe^{2+} + H_2C_2O_4 + 2H_2O \rightarrow FeC_2O_4 \cdot 2H_2O + 2H^+ \qquad (16)$$

Figure 27 shows the potential transient recorded for the dissolution of magnetite under the conditions used to obtain Figure 26.

The transient has a form similar to that obtained in NaEDTA solutions, except region I of Figure 23 is no longer observed. For the first hour or so oxide dissolution occurs at a constant rate, via reaction (15). When oxalate is present, the major potential transition (from region II to III in Figure 23) is no longer smooth. The series of spikes in Figure 27 can be attributed to the opening and repassivation of pores in the base layer. The opening is caused by oxide dissolution. This leads to a surge of $Fe^{2+}$ as metal dissolution occurs at the base of the pores. Repassivation is caused by the precipitation of ferrous ions, via reaction (16). This process of metal exposure/repassivation can be sustained only for a limited time, as more of the pores are opened and eventually the potential transition is completed. In this final region, iron release is in the form of $Fe^{2+}$, mainly from metal dissolution.

At low oxalate concentrations, $\lesssim 10^{-3}$ mol•dm$^{-3}$, not all the oxide is removed prior to the major potential transition. When this occurs the oxide remaining on the surface is difficult to remove just as it was in the absence of oxalate (see above). This suggests that oxide dissolution after the transition is probably via autoreduction, and is again occurring in competition with proton reduction.

There appears to be a change in dissolution mechanism with oxalate concentration. This is illustrated by the data in Figure 28, which shows the oxide and metal dissolution rates calculated from iron release curves similar to those of Figure 26. For oxalate concentrations below $10^{-3}$ mol•dm$^{-3}$, an increase in oxalate concentration accelerates both oxide and metal dissolution rates, and dissolution appears to be occurring via both the direct chemical and autoreductive mechanisms. At higher oxalate concentrations, the oxide dissolution rate is accelerated as the direct chemical mechanism, reaction (15), becomes more important, and the metal dissolution rate is inhibited as ferrous oxalate precipitation occurs, reaction (16).

On the basis of these experiments and others, the following mechanism can be written for the dissolution of magnetite in oxalate-containing solutions, where (►) denotes an atom in the oxide lattice:

(i) Equilibration of the hydrated surface with protons

$$(\blacktriangleright Fe^{III}) - OH + H_3O^+ \rightleftharpoons (\blacktriangleright Fe^{III})^+ + 2H_2O \qquad (17)$$

(ii) Adsorption of oxalate at $Fe^{III}$ sites

$$(\blacktriangleright Fe^{III})^+ + H_2C_2O_4 \rightleftharpoons (\blacktriangleright Fe^{III}C_2O_4)^- + 2H^+ \qquad (18)$$

(iii) Breakdown of the oxide lattice

$$(\blacktriangleright O)^{2-} + 2H_3O^+ \rightarrow 3H_2O \qquad (19)$$

(iv) Desorption of the ferric oxalate species

$$(\blacktriangleright Fe^{III}C_2O_4)^- \rightarrow FeC_2O_4^+ \qquad (20)$$

(v) Removal of ferrous ion from the magnetite lattice

$$(\blacktriangleright Fe^{II}) + 2(\blacktriangleright O)^{2-} + 4H^+ \rightarrow Fe^{2+} + 2H_2O \qquad (21)$$

On the basis of the kinetic data obtained[46], it is difficult to say which of these steps is rate determining. The evidence for adsorption of oxalate on $Fe_3O_4$ was difficult to obtain in the present experiments. However, much evidence exists for oxalate adsorption on other oxide surfaces[47-49], and infrared studies[49] suggest that oxalate is adsorbed on FeOOH by ligand exchange, to form a binuclear bridging complex. If a similar kind of adsorption occurs on magnetite, then the ferric ion dissolution reaction could be written

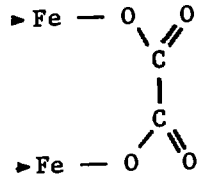


$$+ C_2O_4^{2-} \longrightarrow 2FeC_2O_4^{+} \qquad (22)$$

and would not be a simple, single-step reaction.

Based on the experiments discussed, a number of significant points concerning oxide film dissolution in dilute solutions of complexing agents are apparent:

(i) Dissolution in dilute solutions at low temperatures is inefficient and involves some metal dissolution, leading to a small chance of pitting.

(ii) The oxide dissolution rate is not necessarily proportional to the complexing ability of the anion.

(iii) The morphology and porosity of the surface films are very important in determining the kinetics of oxide dissolution.

(iv) Oxalic acid accelerates oxide dissolution but not by acting as a reducing agent.

These conclusions, along with others based on loop experiments of a more applied nature are extremely valuable in choosing the optimum reagents and operating conditions for removing boiler circuit corrosion films (and the associated radionuclides) without significant corrosion of the structural materials.

## 4. CONCLUSION

An understanding of the basic mechanisms of film growth and dissolution has proved valuable in characterizing a large number of corrosion problems in the nuclear industry. A number of these problems, and some of the work undertaken to solve them, have been described. In many cases the understanding obtained has proved of major value in developing solutions to these problems.

## REFERENCES

1. L. Young, Anodic Oxide Films, Academic Press, New York, 1961.

2. D.A. Vermilyea, "Anodic Films", in Advances in Electrochemistry and Electrochemical Engineering, Vol. 3, P. Delahay and C.W. Tobias, eds., Interscience, New York, 1963.

3. L. Young, W.S. Goruk and F.G.R. Zobel, "Ionic and Electronic Currents at High Fields in Anodic Oxide Films", in Modern Aspects of Electrochemistry, Vol. 4, J.O'M. Bockris, ed., Butterworths, London, 1966.

4. M.J. Dignam, "The Kinetics of the Growth of Oxides", in Comprehensive Treatise of Electrochemistry, Vol. 4, J. O'M. Bockris, B.E. Conway, E. Yeager and R.E. White, eds., Plenum Press, New York, 1981.

5. L. Gainer and G. Wallwork, "A Review of Pitting Corrosion Theories", Rev. on Coat. Corros. 3, 49 (1978).

6. Z. Szklarska-Smialowska, "Review of Literature on Pitting Corrosion Published Since 1960", Corrosion 27, 223 (1971).

7. H.J. Engell, "Stability and Breakdown Phenomena of Passivating Films", Electrochim. Acta 22, 987 (1977).

8. R.G. Barradas, K. Belinko and D.W. Shoesmith, "Study of Surface Effects in the Formation of Lead Chloride on Lead Electrodes in Aqueous HCl by Electrochemical Methods and Scanning Electron Microscopy", Electrochim. Acta 21, 357 (1976).

9. D.W. Shoesmith and Woon Lee, "The Dissolution of Cupric Hydroxide Films from Copper Surfaces", Electrochim. Acta 22, 1411 (1977).

10. S. Sunder, D.W. Shoesmith, M.G. Bailey and F.W. Stanchell, "Anodic Oxidation of $UO_2$ Part I. Electrochemical and X-Ray Photoelectron Spectroscopic Studies in Neutral Solutions", J. Electroanal. Chem. 130, 163 (1981).

11. J. Boulton, ed., "Management of Radioactive Fuel Wastes: The Canadian Disposal Program", Atomic Energy of Canada Limited Report, AECL-6314 (1978).

12. T.T. Vandergraaf, L.H. Johnson and D.W.P. Lau, "Leaching of Irradiated CANDU $UO_2$ Fuel", in Scientific Basis for Nuclear Waste Management, Vol. 2, p. 335, C.J.M. Northrup, Jr., ed., Plenum Press, New York, 1980.

13. L.H. Johnson, D.W. Shoesmith, G.E. Lunansky, M.G. Bailey, and P.R. Tremaine, "Mechanisms of Leaching and Dissolution of $UO_2$ Fuel", Nucl. Tech. 56, 2388 (1982).

14. R.J. Lemire and P.R. Tremaine, "Uranium and Plutonium Equilibria in Aqueous Solutions to 200°C", J. Chem. Eng. Data 25, 361 (1980).

15. J. Paquette and R.J. Lemire, "A Description of the Chemistry of Aqueous Solutions of Uranium and Plutonium to 200°C Using Potential-pH Diagrams", Nucl. Sci. Eng. 79, 26 (1981).

16. P.R. Tremaine, J.D. Chen, G. Wallace and W.A. Boivin, "The Solubility of Uranium (IV) Oxide in Alkaline Aqueous Solutions to 300°C", J. Solution Chem. 10, 221 (1981).

17. M.J. Nicol and C.R.S. Needes, "The Anodic Dissolution of Uranium Dioxide - I. In Perchlorate Solutions", Electrochim. Acta 20, 585 (1975).

18. M.J. Nicol and C.R.S. Needes, "The Anodic Dissolution of Uranium Dioxide - II. In Carbonate Solutions", Electrochim. Acta 22, 1381 (1977).

19. N.S. McIntyre, S. Sunder, D.W. Shoesmith and F.W. Stanchell, "Chemical Information from XPS - Applications to the Analysis of Electrode Surfaces", J. Vac. Sci. Tech., 18, 714 (1981).

20. I.J. Hastings, D.H. Rose and J. Baird, "Identification of Precipitates Associated with Intergranular Fission Gas Bubbles in Irradiated $UO_2$ Fuel", J. Nucl. Mater. 61, 229 (1976).

21. H.K. Rae, "Chemical Exchange Processes for Heavy Water", Atomic Energy of Canada Limited Report, AECL-2555, (1966).

22. L.R. Haywood and P.B. Lumb, "The Heavy Water Industry", Chem. Can. 27, 29 (1975).

23. G.F. Taylor, "The Corrosion of Steel in Heavy Water Production-Operating Experience and Laboratory Development", presented at the 7th International Congress of Metallic Corrosion, Rio de Janeiro, Brazil, 1978, Oct. 4-11.

24. G.F. Taylor, unpublished data.

25. P.H. Tewari, G. Wallace and A.B. Campbell, "The Solubility of Iron Sulphides and Their Role in Mass Transport in Girdler-Sulphide Heavy Water Plants", Atomic Energy of Canada Limited Report, AECL-5960 (1977).

26. D.W. Shoesmith, M.G. Bailey and B. Ikeda, "Electrochemical Formation of Mackinawite in Alkaline Sulphide Solutions", Electrochim. Acta 23, 1329 (1978).

27. D.W. Shoesmith, P. Taylor, M.G. Bailey and D.G. Owen, "The Formation of Ferrous Monosulphide Polymorphs During the Corrosion of Iron by Aqueous Hydrogen Sulphide at 21°C", J. Electrochem. Soc. 127, 1007 (1980).

28. A.G. Wikjord, T.E. Rummery, F.E. Doern and D.G. Owen, "Corrosion and Deposition During the Exposure of Carbon Steel to Hydrogen Sulphide-Water Solutions", Corros. Sci. 20, 651 (1980).

29. P. Taylor, T.E. Rummery and D.G. Owen, "On the Conversion of Mackinawite to Greigite", J. Inorg. Nucl. Chem. 41, 595 (1979).

30. P. Taylor, T.E. Rummery and D.G. Owen, "Reactions of Iron Monosulphide Solids with Aqueous Hydrogen Sulphide up to 160°C", J. Inorg. Nucl. Chem. 41, 1683 (1979).

31. P. Taylor, "The Stereochemistry of Iron Sulphides - A Structural Rationale for the Crystallization of Some Metastable Phases from Aqueous Solution", Amer. Mineral. 65, 1026 (1980).

32. P.H. Tewari, M.G. Bailey and A.B. Campbell, "The Erosion-Corrosion of Carbon Steel in Aqueous $H_2S$ Solutions up to 120°C and 1.6 MPa Pressure", Corros. Sci. 19, 573 (1979).

33. D.W. Shoesmith, T.E. Rummery, M.G. Bailey and D.G. Owen, "Electrocrystallization of Pyrite and Marcasite on Stainless Steel Surfaces", J. Electrochem. Soc. 126, 911 (1979).

34. P.H. Tewari and A.B. Campbell, "Dissolution of Iron Sulphide (Troilite) in Aqueous Sulfuric Acid", J. Phys. Chem. 80, 1844 (1976).

35. P.H. Tewari and A.B. Campbell, "Dissolution of Iron During the Initial Corrosion of Carbon Steel in Aqueous $H_2S$ Solutions", Can. J. Chem. 57, 188 (1979).

36. A.G. Wikjord, T.E. Rummery and F.E. Doern, "Crystallization of Pyrite from Deoxygenated Aqueous Sulphide Solutions at Elevated Temperature and Pressure", Can. Mineral. 14, 571 (1976).

37. D.W. Shoesmith, T.E. Rummery, M.G. Bailey and D.G. Owen, "Electrochemical Formation of Sulfur at Stainless Steel Surfaces", J. Electrochem. Soc. 127, 27 (1980).

38. K.A. Burrill, "A Possible Mechanism for Corrosion Product Transport and Radiation field Growth in a Pressurized Water Reactor Primary Circuit", Nucl. Tech. 36, 85 (1977).

39. D.H. Lister, "The Transport of Radioactive Corrosion Products in High Temperature Water. II - Activation of Isothermal Steel Surfaces", Nucl. Sci. Eng. 59, 406 (1976).

40. D.H. Lister, "The Accumulation of Radioactive Corrosion Products in Nuclear Steam Generators", Corrosion 35, 219 (1979).

41. P.J. Pettit, J.E. Lesurf, W.B. Stewart, R.J. Strickert and S.B. Vaughan, "Decontamination of the Douglas Point Reactor by the Can-Decon Process", Mater. Perform. 19, 34 (1980).

42. J.A. Ayres, Decontamination of Nuclear Reactors and Equipment, Ronald Press, New York, 1970.

43. D.W. Shoesmith, T.E. Rummery, Woon Lee and D.G. Owen, "Dissolution of Oxide Films on Iron in Aqueous Solutions Containing Complexing Anions - I. Magnetite in Citrate and Ethylenediaminetetraacetate", Power Ind. Res. 1, 43 (1981).

44. J.E. Castle and G.M.W. Mann, "The Mechanism of Formation of a Porous Oxide Film on Steel", Corros. Sci. 6, 253 (1966).

45. J.E. Castle and H.G. Masterson, "The Role of Diffusion in the Oxidation of Mild Steel in High-Temperature Aqueous Solutions", Corros. Sci. 6, 93 (1966).

46. D.W. Shoesmith, Woon Lee and D.G. Owen, "Dissolution of Oxide Films on Iron in Aqueous Solutions Containing Complexing Anions - II. Magnetite in Oxalic Acid plus EDTA", Power Ind. 1, 253 (1981).

47. G. Koch, "Kinetics and Mechanism of the Solution of Beryllium Oxide in Acids", Ber. Bunsenges. Phys.Chem. 69, 141 (1965).

48. H. Yoneyama, T. Fujimoto, K. Kubo and H. Tamura, "Adsorption of Dicarboxylic Acids on Lithiated Nickel Oxide Electrodes", J. Electroanal. Chem. 63, 85 (1975).

49. R.L. Parfitt and J.D. Russell, "Adsorption on Hydrous Oxides. IV Mechanisms of Adsorption of Various Ions on Goethite", J. Soil Sci. 28, 297 (1977).

TABLE 1

EXAMPLES OF MULTILAYER FILMS

| SYSTEM | GROWTH CONDITIONS | FILM PRODUCED | |
|---|---|---|---|
| | | BASE LAYER | PRECIPITATED LAYER |
| Cu/LiOH | Constant Potential in 1 mol.dm$^{-3}$ LiOH | $Cu_2O$ | $Cu(OH)_2$ ($T < 35^oC$)<br>CuO ($T > 35^oC$) |
| Fe/$H_2S$(aq) | (i) Constant Current<br>(ii) Natural Corrosion<br>$p_{H_2S}$ = 2MPa | $FeS_{1-x}$<br>$FeS_{1-x}$ | $FeS_{1-x}$;$(FeS)_c$;$(FeS)_t$<br>$FeS_{1-x}$;$(FeS)_c$;$(FeS)_t$;<br>$FeS_{1+x}$;$(FeS_2)_p$;$(FeS_2)_m$ |
| Fe/NaOH | Corrosion 280$^oC$<br>(i) $p_{H_2}$ = 15 kPa<br>(ii) $p_{H_2}$ = 0 | $Fe_3O_4$<br>$Fe_3O_4$ | $Fe_3O_4$<br>$Fe_2O_3$ |
| $UO_2$/$Na_2SO_4$ | Constant Potential<br>0.5 mol.dm$^{-3}$ $Na_2SO_4$;<br>pH = 6 to 10.5 | $UO_{2+x}$;$U_3O_7$;<br>$U_2O_5$;$U_3O_8$ | $UO_3.xH_2O$ |

TABLE 2

IRON SULPHIDE NOMENCLATURE

| | |
|---|---|
| Near FeS | Mackinawite, $FeS_{1-x}$; Troilite*,$(FeS)_t$;<br>Cubic Ferrous Sulphide, $(FeS)_c$;<br>Pyrrhotites*; $FeS_{1+x}$ |
| Near $Fe_3S_4$ | Greigite, Smythite |
| $FeS_2$ | Pyrite* $(FeS_2)_p$; Marcasite $(FeS_2)_m$ |

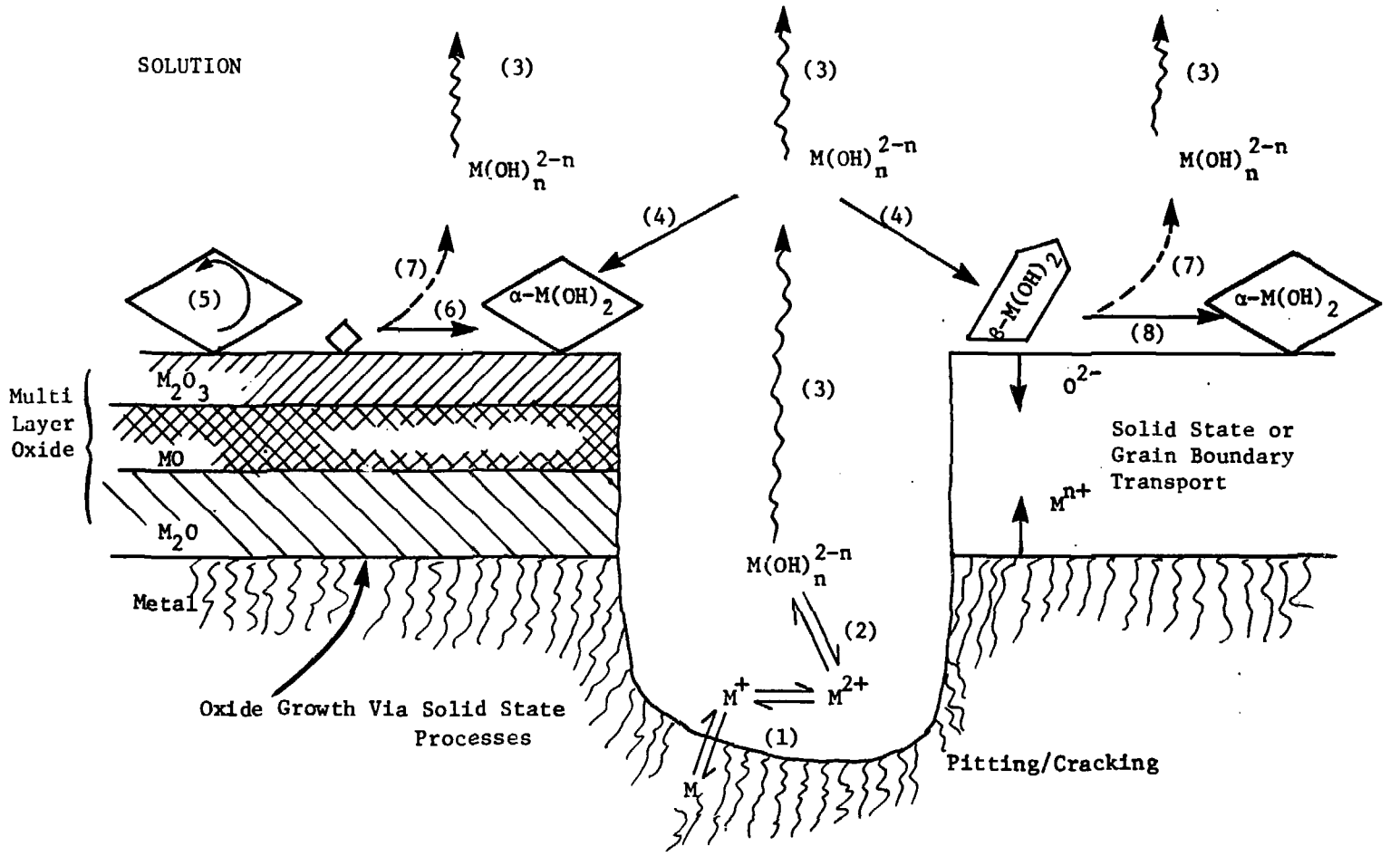


(1) Metal dissolution
(2) Hydrolysis
(3) Transport (diffusion/convection)
(4) Precipitation
(5) Solid state conversion
(6) Ostwald ripening
(7) Oxide dissolution
(8) Dissolution - Reprecipitation

FIGURE 1: Mechanisms of Film Growth and Dissolution

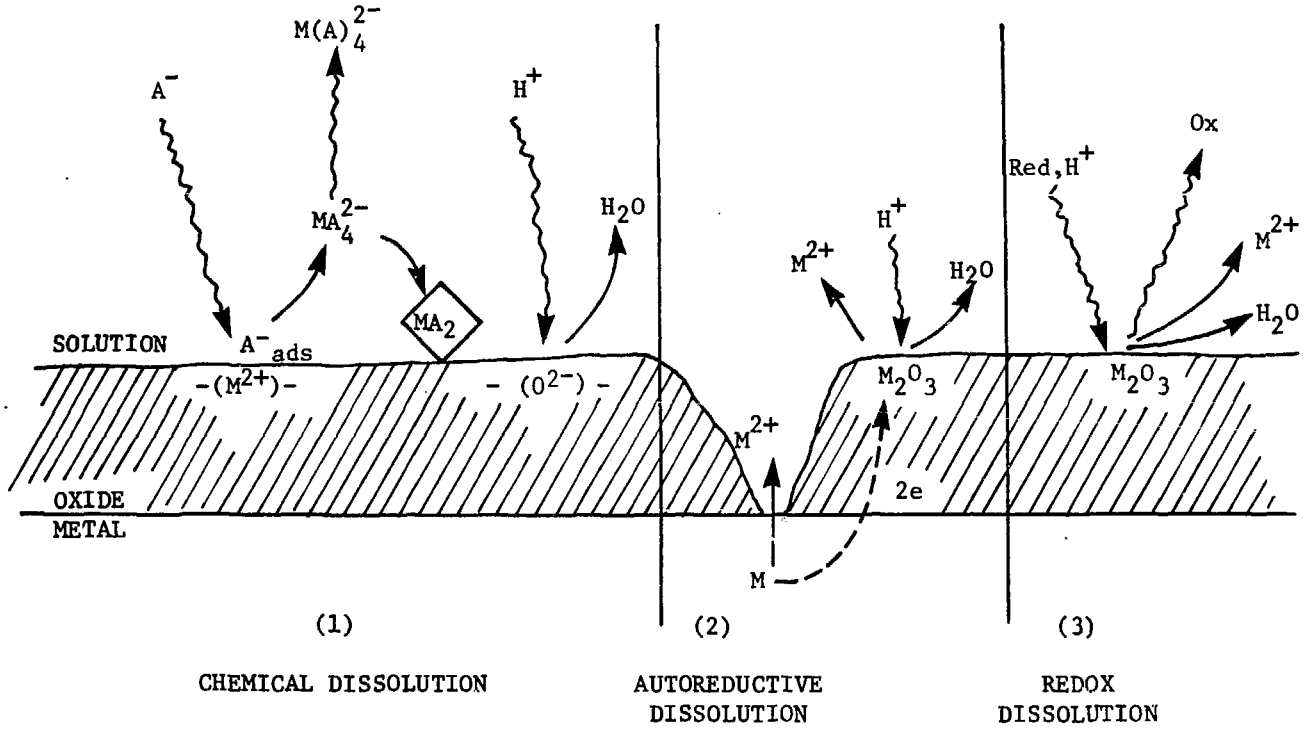


FIGURE 2: Possible Dissolution Mechanisms for Films on Metal Surfaces

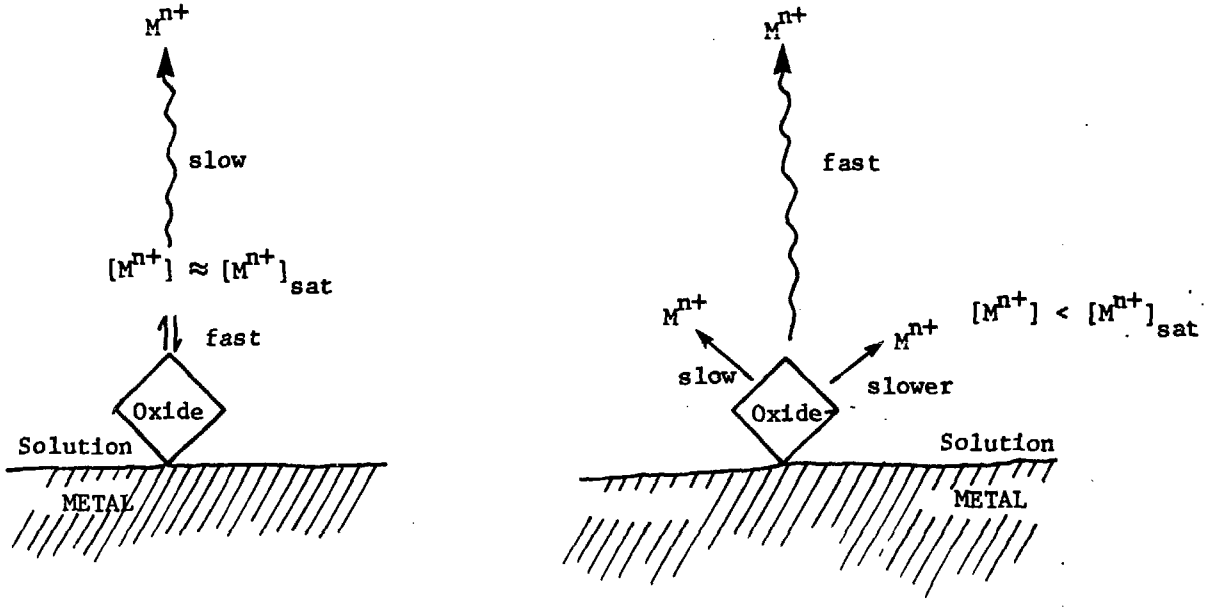


A. TRANSPORT CONTROL

No Crystallographically Controlled Surface Features

B. SURFACE - REACTION CONTROL

Selective Dissolution of Crystal Faces Occurs

FIGURE 3: Microscopic Examination of Surface Morphology as an Indicator of Rate Controlling Mechanism for Dissolution

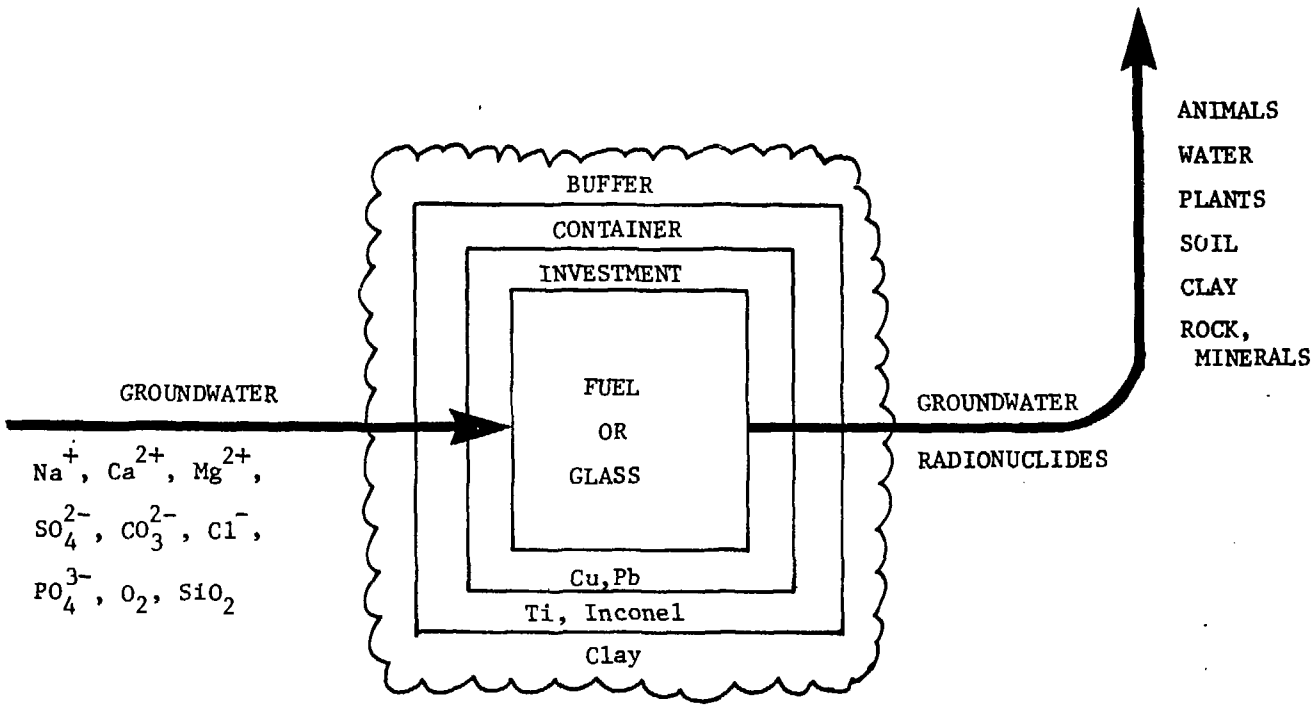


FIGURE 4: Schematic of a Waste Repository

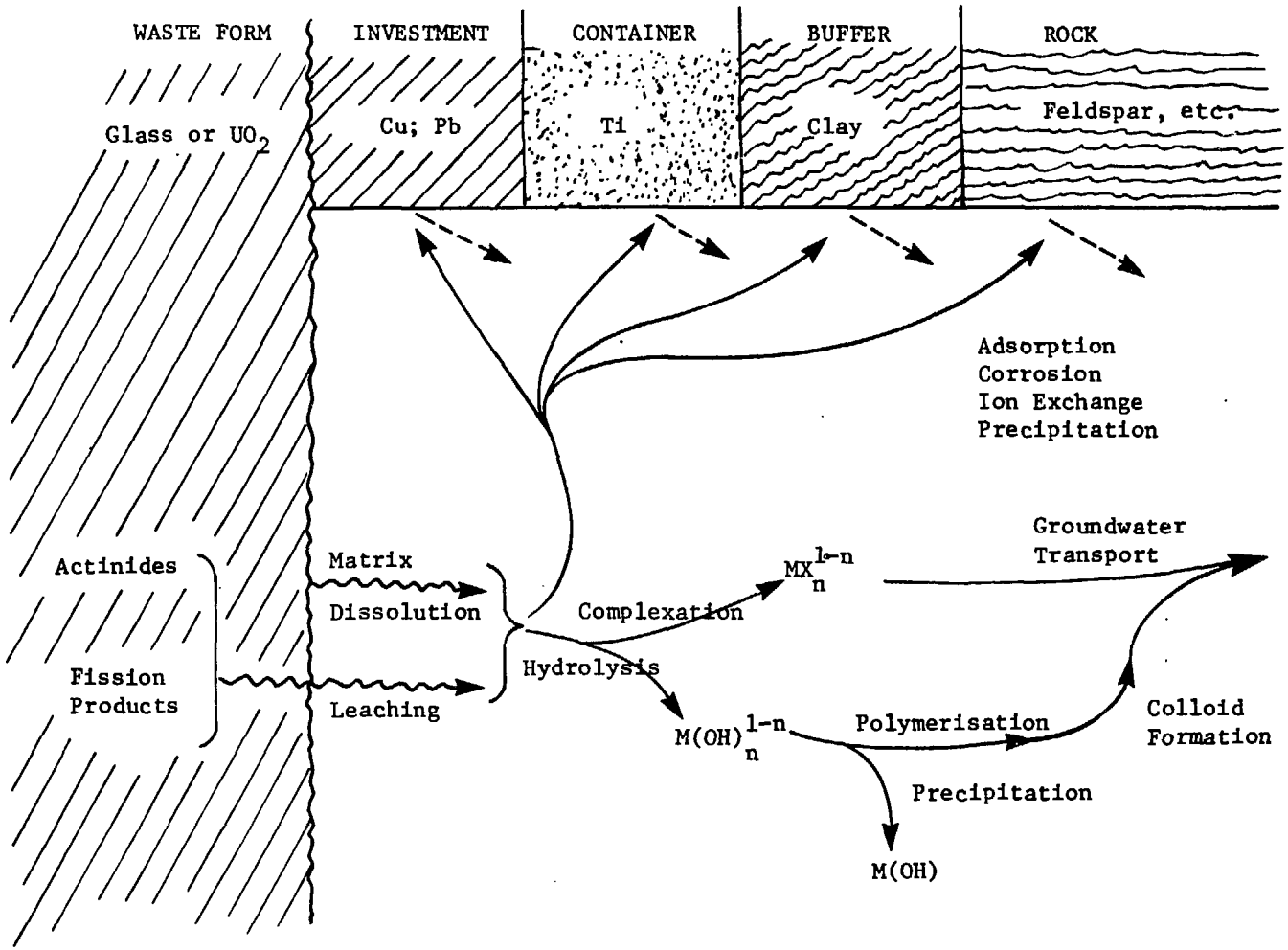


FIGURE 5: Possible Interactions in a Waste Repository

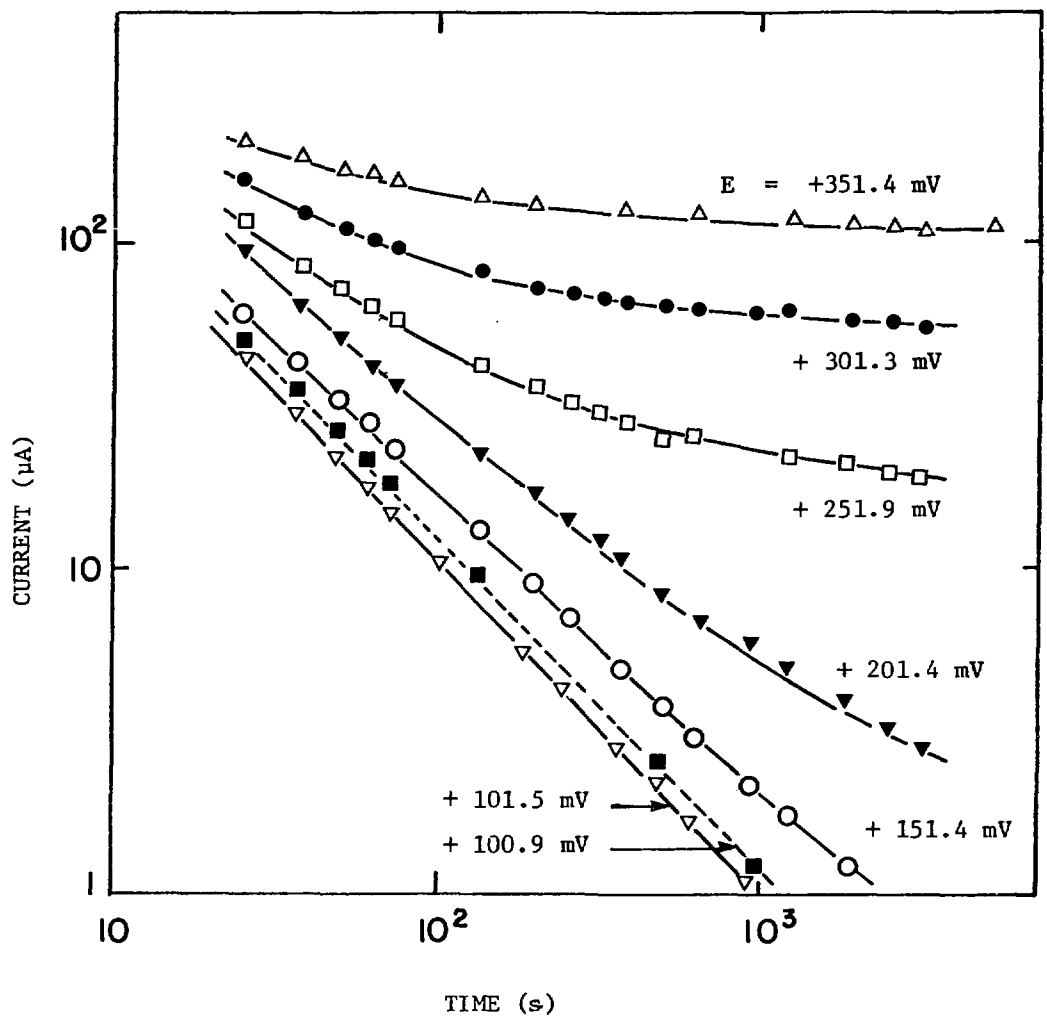


FIGURE 6: Potentiostatic Oxidation of $UO_2$ in 0.5 mol.dm$^{-3}$ $Na_2SO_4$, pH = 3.8, as a Function of Potential. Electrode repolished between runs.

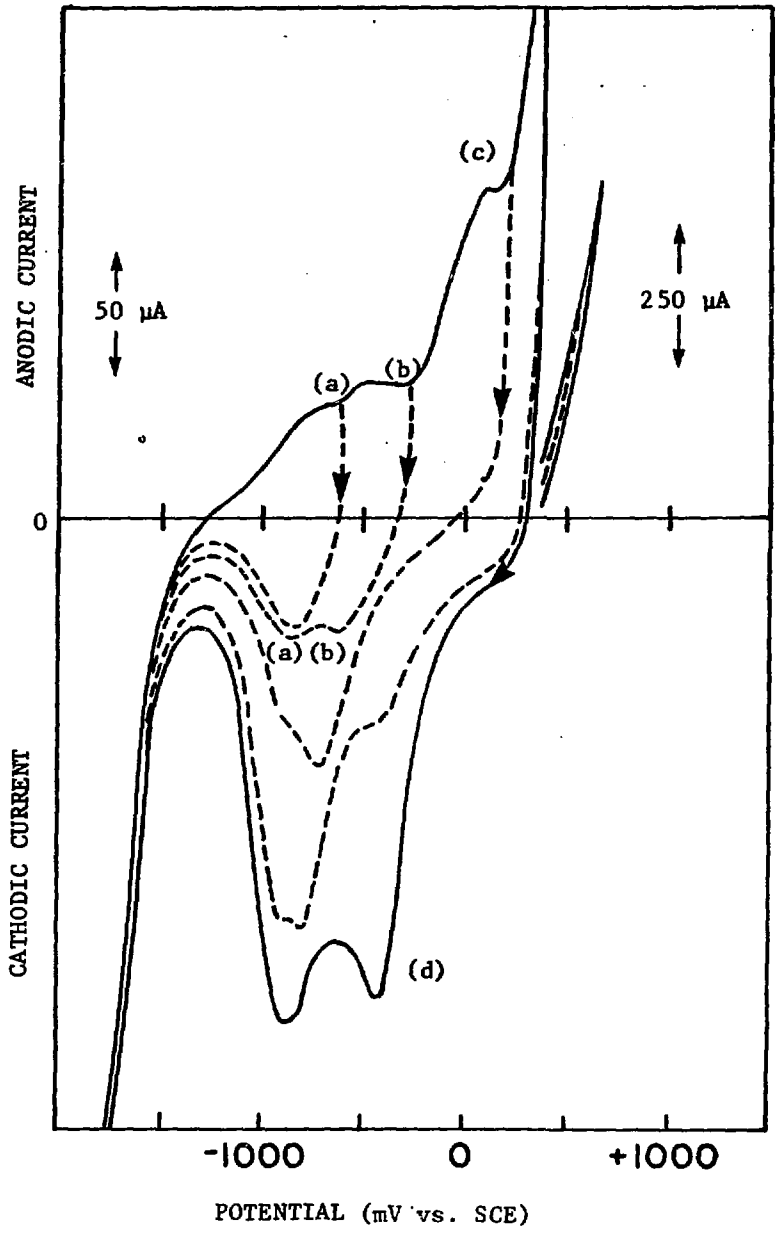


FIGURE 7: Cyclic Voltammograms to Various Anodic Potential Limits at 20 $mV.s^{-1}$ in 0.5 $mol.dm^{-3}$ $Na_2SO_4$; pH ≈ 10.5

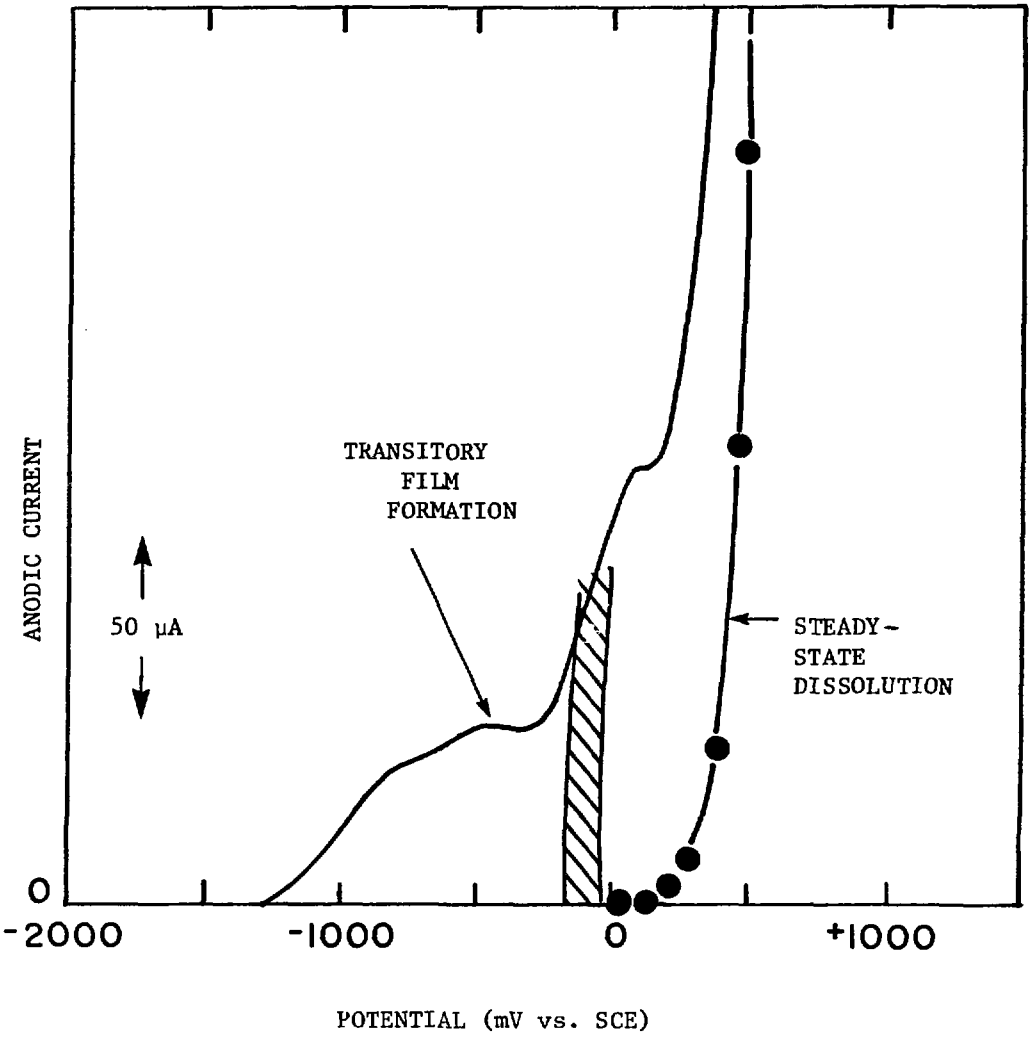


FIGURE 8: Anodic Sweep of Figure 7 ($20.\ mV.s^{-1}$) and Steady-State Currents Recorded on $UO_2$ in 0.5 $mol.dm^{-3}$ $Na_2SO_4$; pH = 10.5

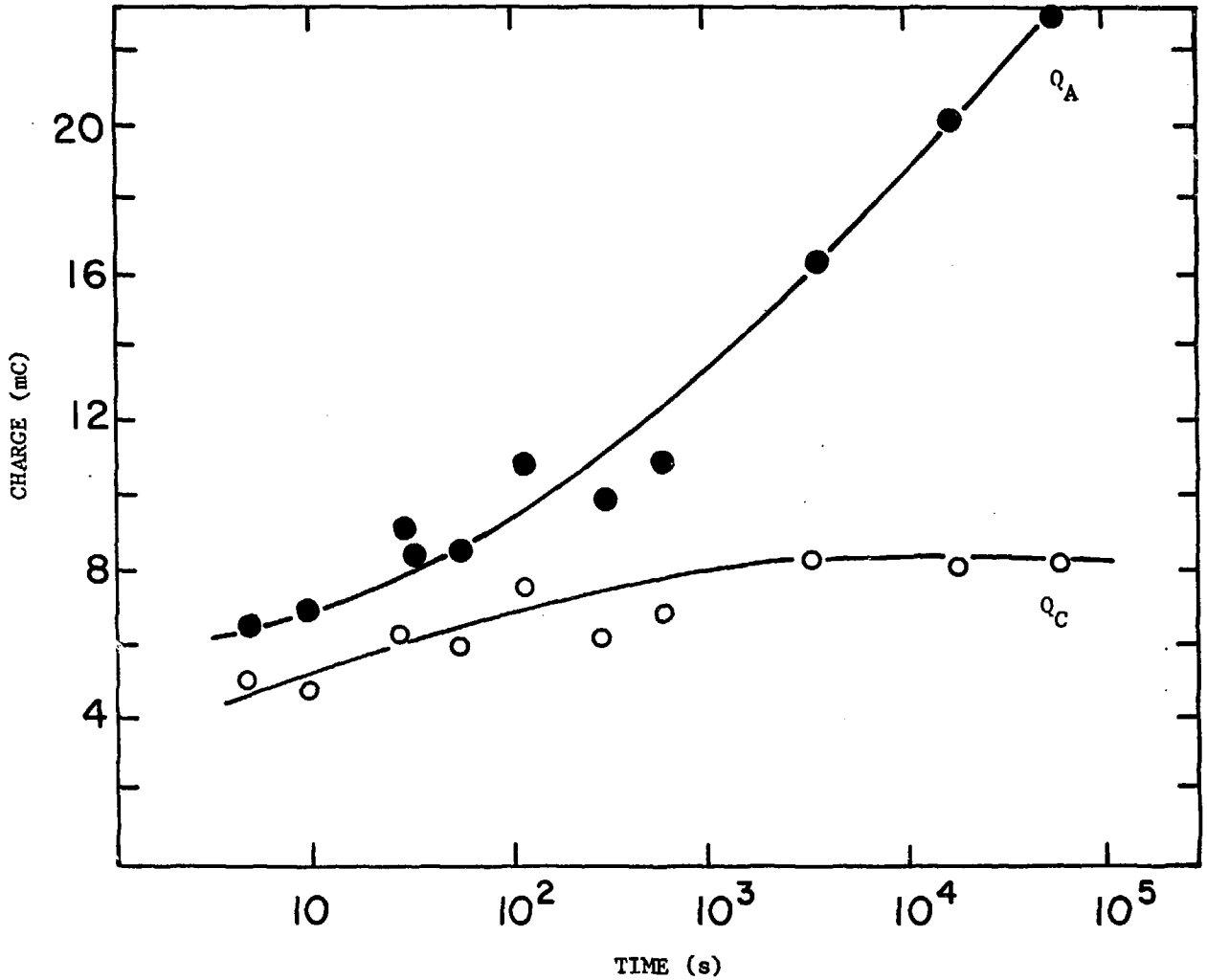


FIGURE 9: Total Anodic Charge ($Q_A$) and the Charge Associated with Film Formation ($Q_C$) for Potentiostatic Film Growth at E = 202 mV (vs. SCE) for Varying Times in 0.5 mol.dm$^{-3}$ $Na_2SO_4$; pH = 9

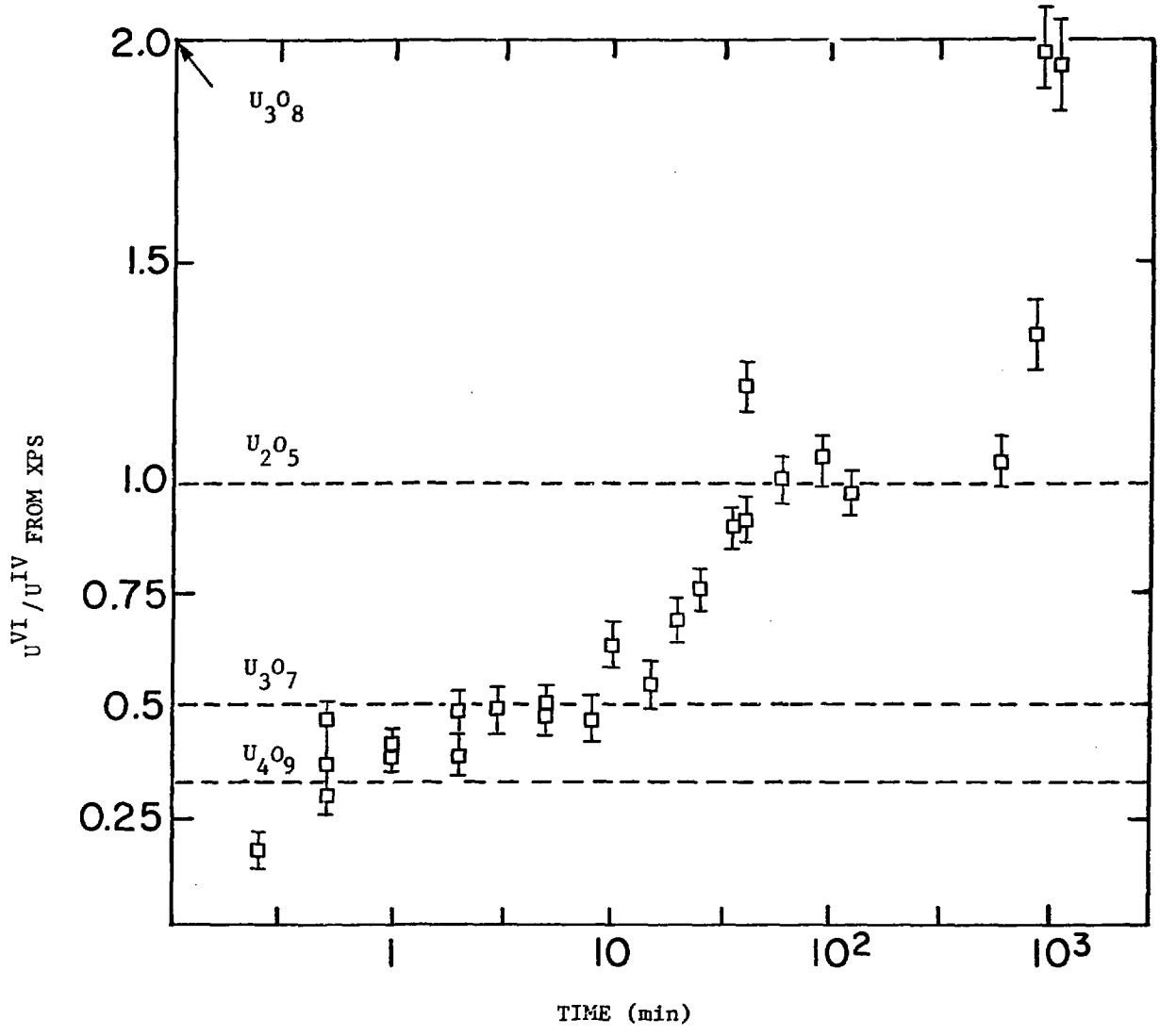


FIGURE 10: Changes in Stoichiometry of $UO_2$ Electrode Surface During Potentiostatic Oxidation at +300 mV in 0.5 mol.dm$^{-3}$ $Na_2SO_4$, pH = 7, as a Function of Oxidation Time. Error bars refer to the limiting precision of the $U^{VI}$ to $U^{IV}$ ratio resulting from errors in the deconvolution of the U-4$f_{7/2}$ X-ray photoelectron spectral band.

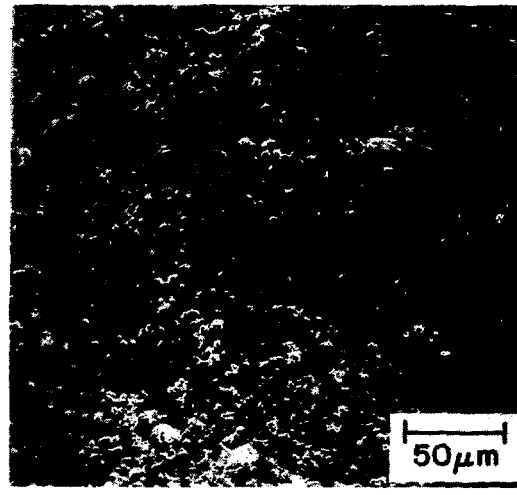


A. ORIGINAL SURFACE

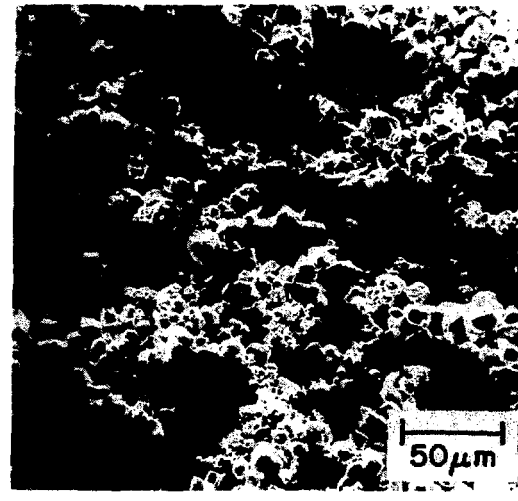


B. SURFACE AFTER 78 DAYS

FIGURE 11: Surface of a $UO_2$ Electrode Before and After 78 Days of Constant Current Dissolution (10μA) in 0.5 mol.dm$^{-3}$ $Na_2SO_4$ + 0.01 mol.dm$^{-3}$ $Na_2CO_3$

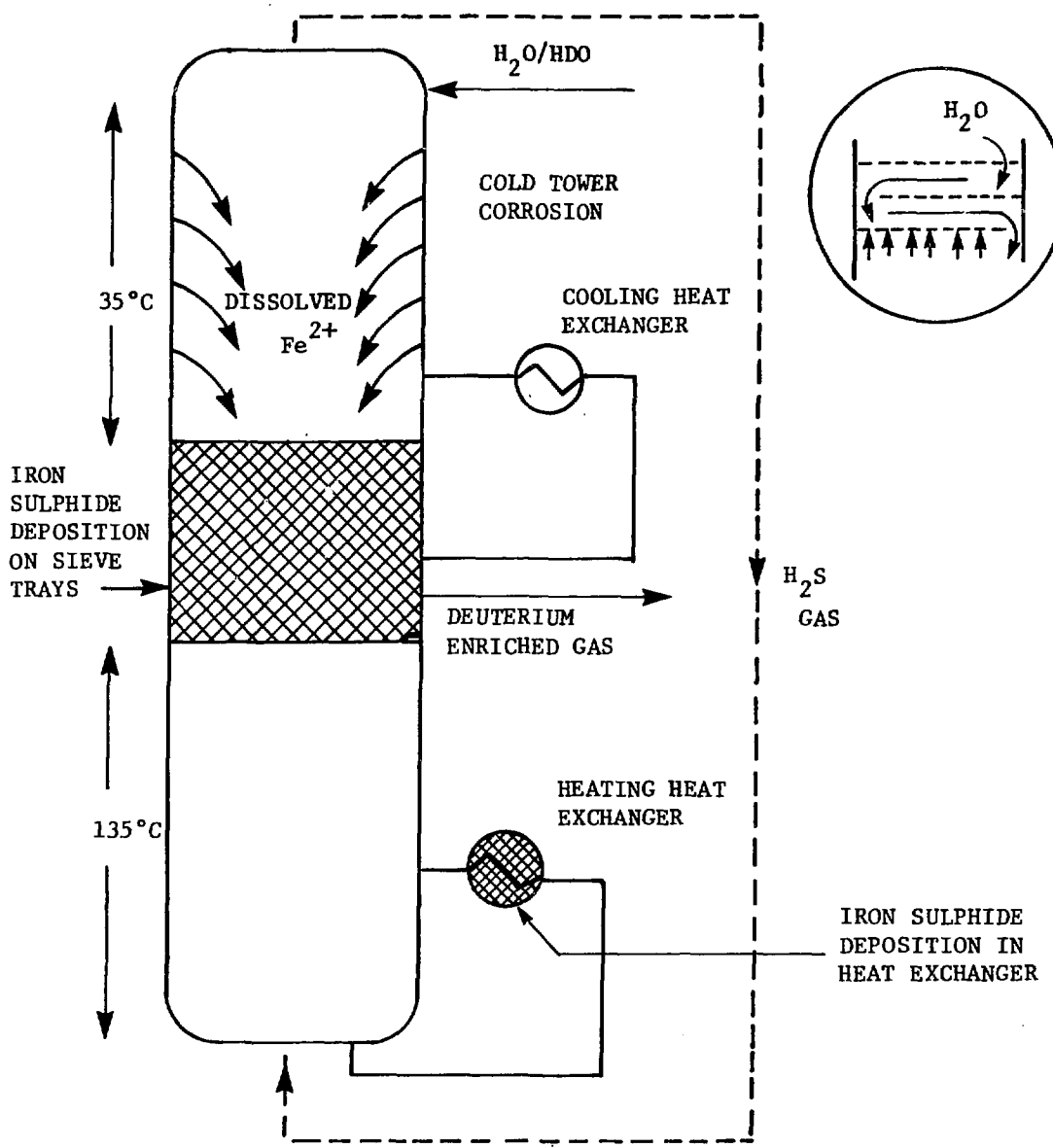


FIGURE 12: Carbon-Steel Corrosion and Iron Sulphide Deposition in Heavy-Water Plant Enriching Units

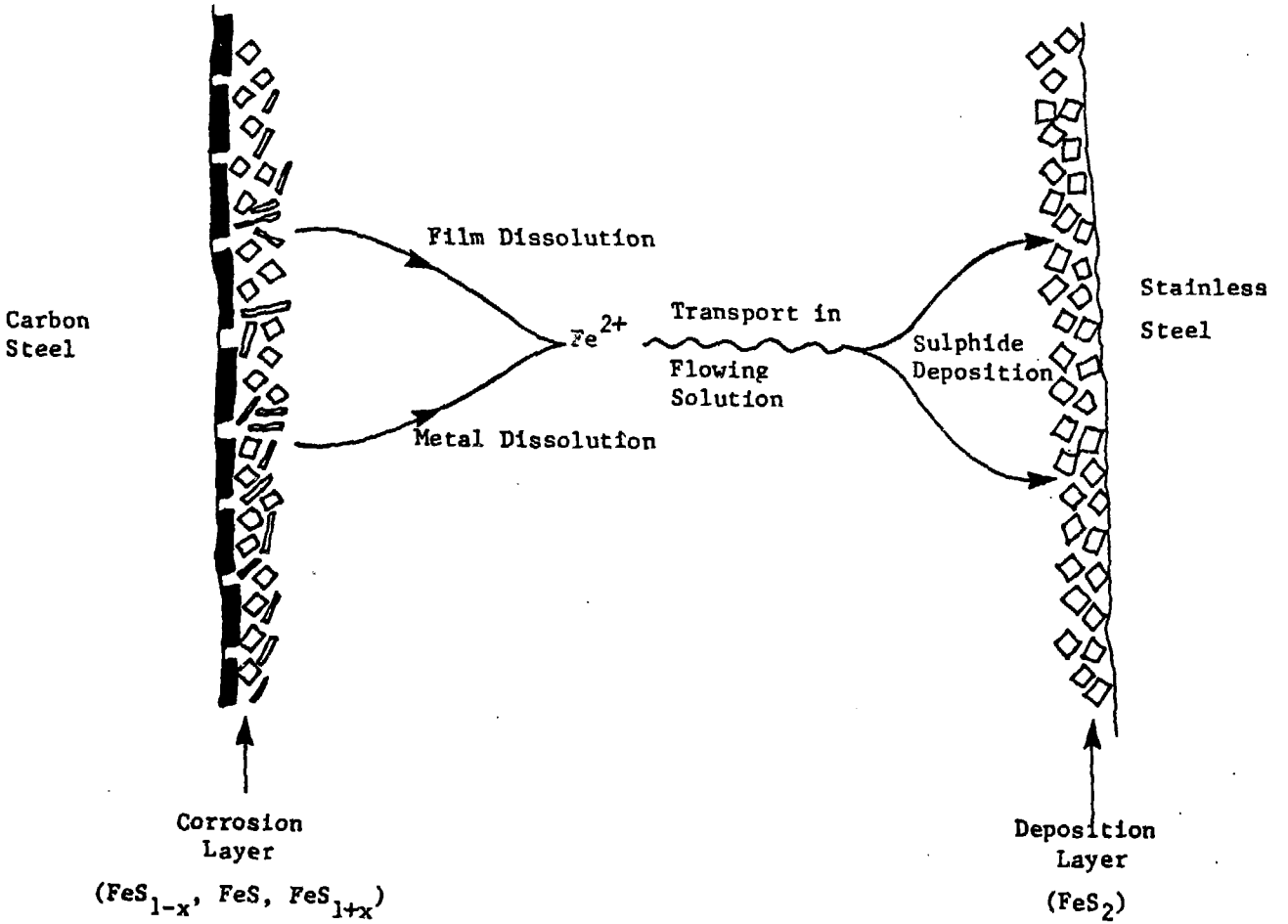


**FIGURE 13:** Transport of Soluble Iron from Corroding Carbon-Steel Surfaces to Non-corroding Stainless-Steel Surfaces

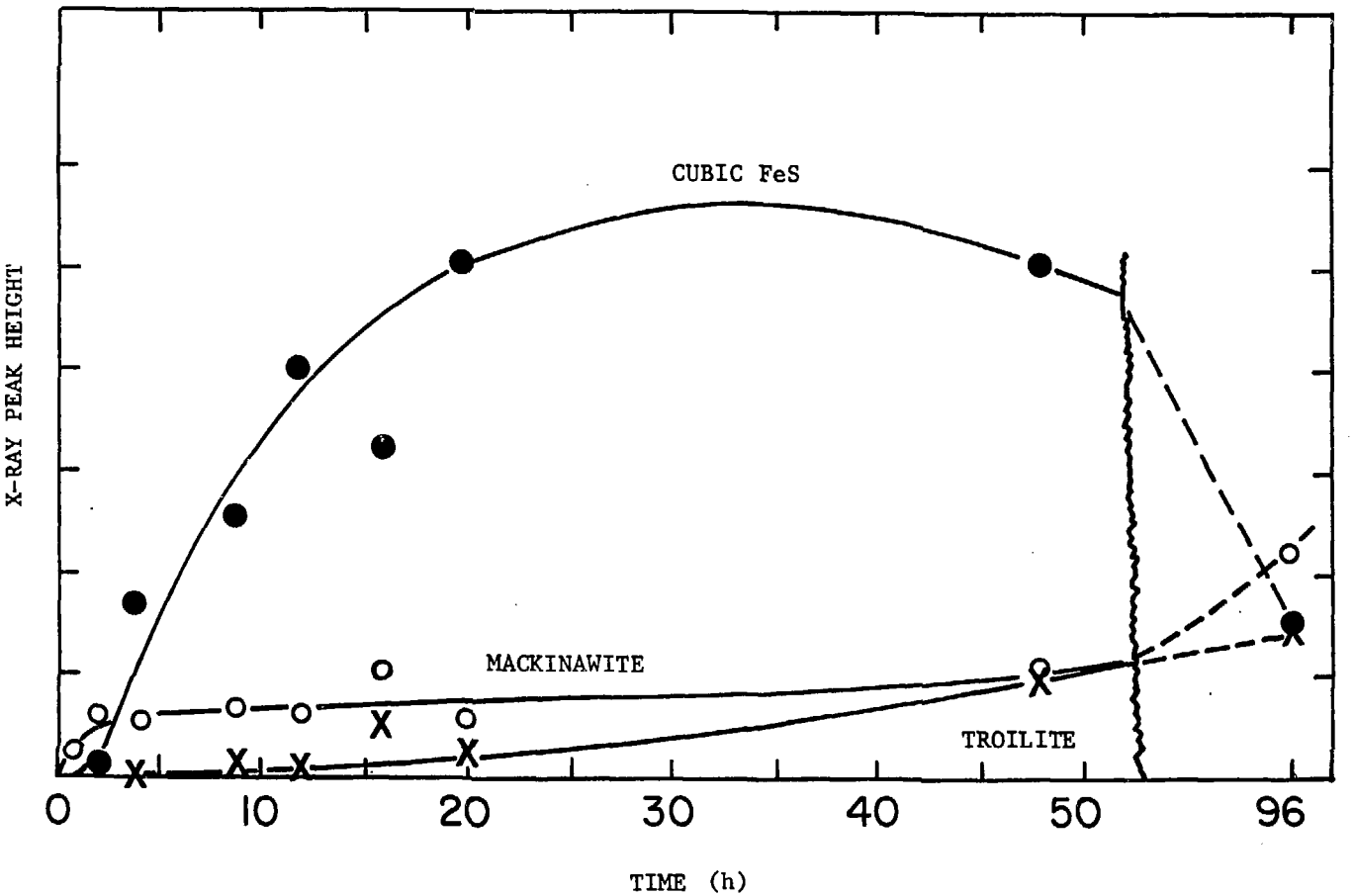


FIGURE 14: Relative Amounts of Iron Sulphide Phases Formed on Iron Surfaces Exposed to Saturated Aqueous $H_2S$ Solution at 21°C and pH = 4 as a Function of Time

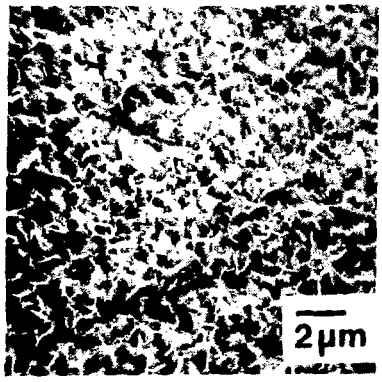


0.5 h

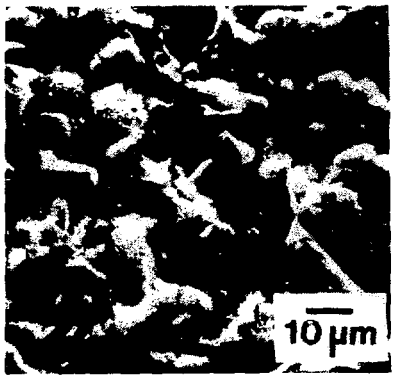


1.0h

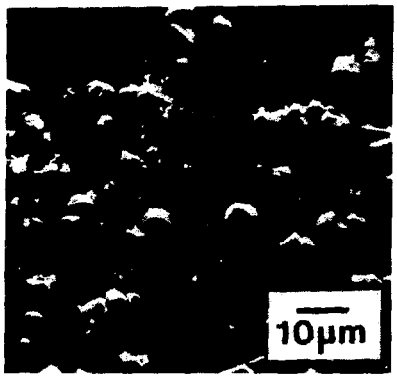


4h

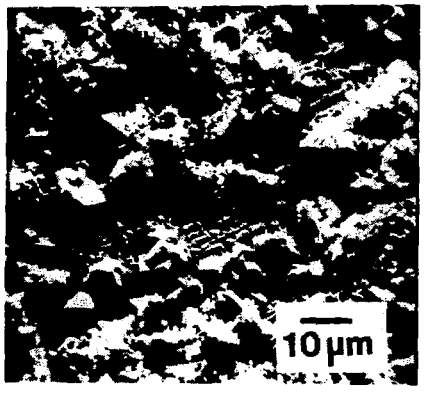


12h

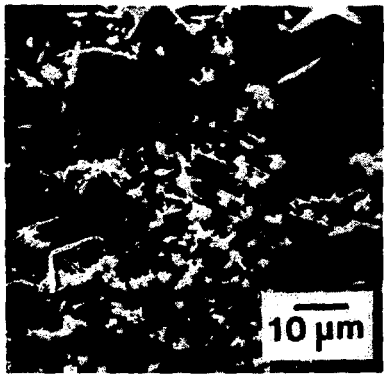


16h


24h

FIGURE 15: Scanning Electron Micrographs of Iron Surfaces Exposed to Saturated Aqueous $H_2S$ Solution at 21°C and pH = 4 for Various Times

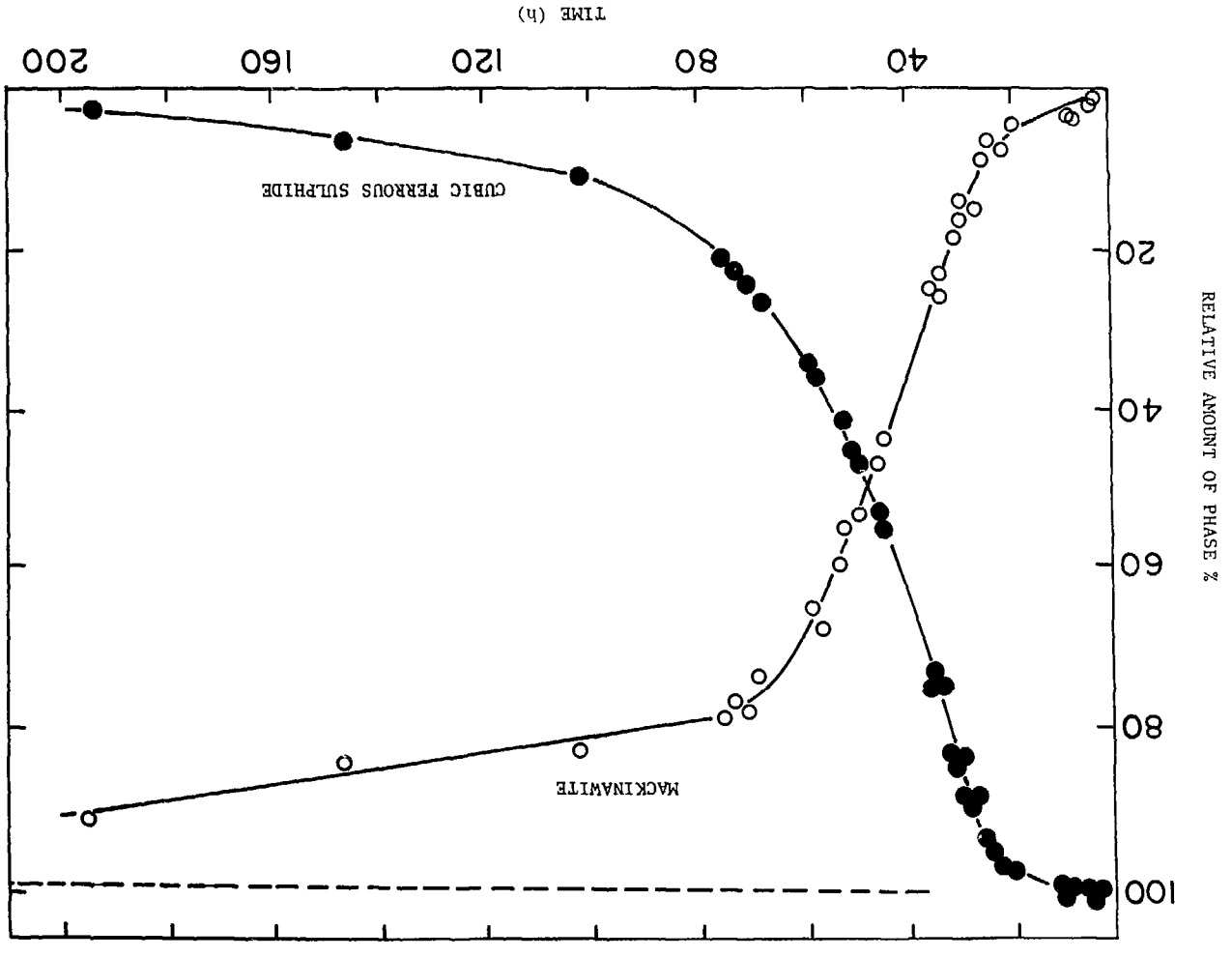


FIGURE 16: Relative Amounts of Cubic Ferrous Sulphide and Mackinawite During Interconversion at 21°C as Determined by X-ray Diffractometry

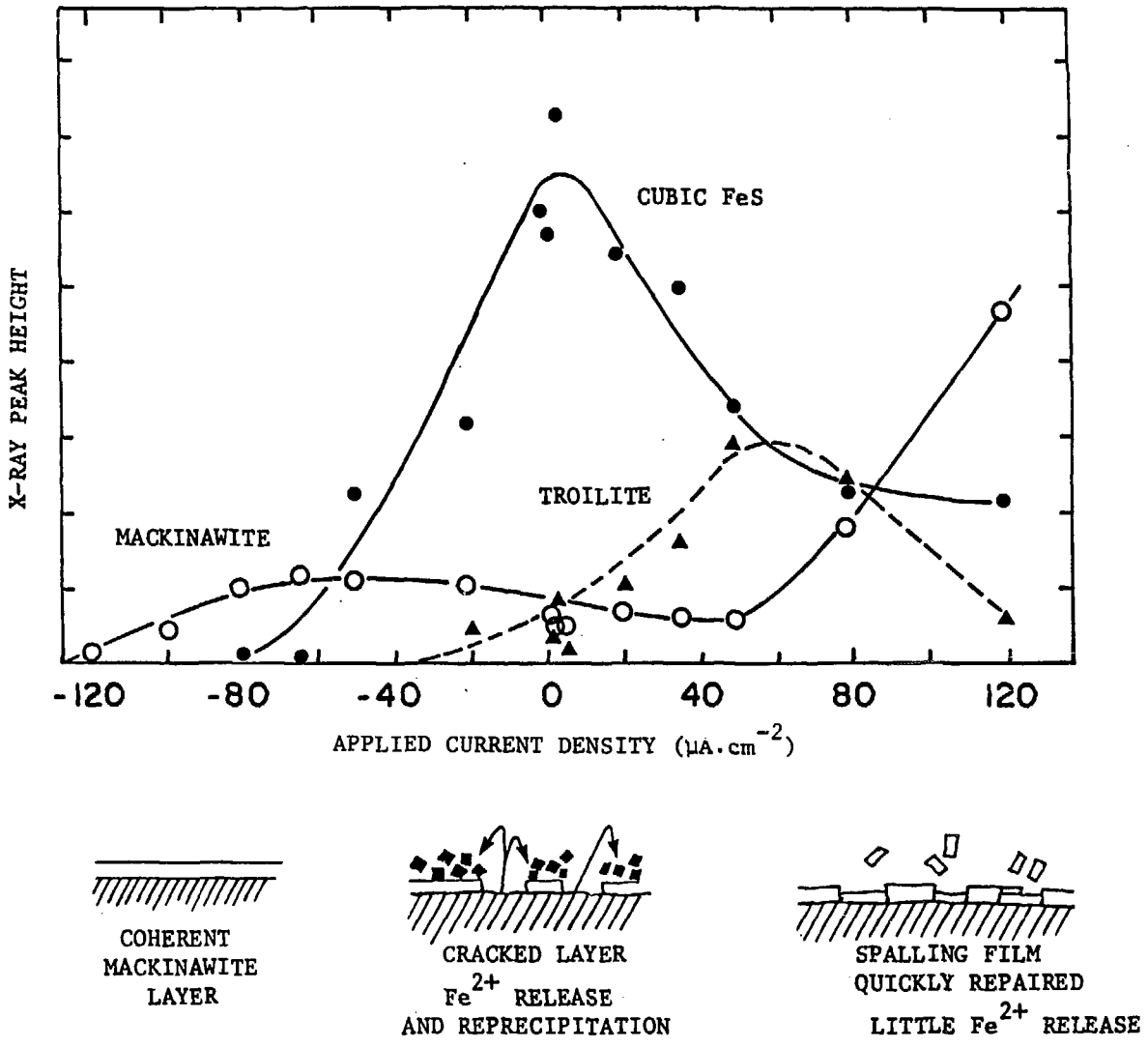


FIGURE 17: Relative Amounts of Iron Sulphide Phases Formed on Iron Surfaces Exposed to Saturated Aqueous $H_2S$ Solution at 21°C and pH = 4 for 24 Hours as a Function of Applied Current Density

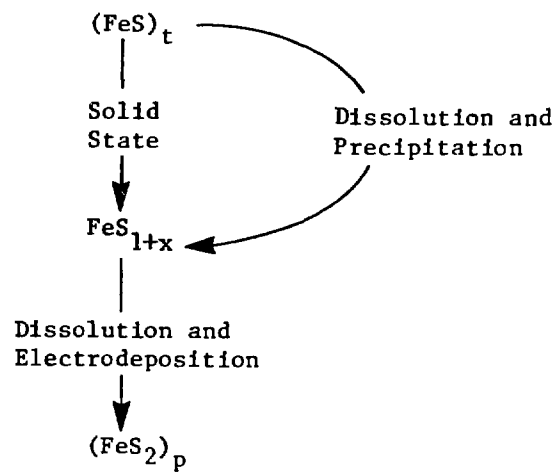


(a) INCREASING TEMPERATURE

Reaction sequence accelerated, especially for $T \gtrsim 100^{\circ}C$

(b) INCREASING $H_2S$ PRESSURE

| | | |
|---|---|---|
| $(FeS)_t$ | → $FeS_{1+x}$ | - effect uncertain |
| $FeS_{1+x}$ | → $(FeS_2)_p$ | - accelerated |

(c) STIRRING

| | | |
|---|---|---|
| $(FeS)_t$ | → $FeS_{1+x}$ | - partially affected |
| $FeS_{1+x}$ | → $(FeS_2)_p$ | - prevented |

(d) PRESENCE OF AN ANODIC SINK (e.g. stainless steel)

| | | |
|---|---|---|
| $FeS_{1+x}$ | → $(FeS_2)_p$ | - prevented |

FIGURE 18: Effect of Some Variables on the Rate of Transformation of Troilite to Pyrrhotite and Pyrite

FIGURE 19: Troilite Single Crystal Face After Exposure to Aqueous $H_2S$ at 130°C for Six Days, in Close Proximity to a Titanium Surface. Note the severe etching at left-hand side and dense, highly crystalline pyrite deposit, with gradation of crystal size towards the edge of the face (courtesy of P. Taylor).

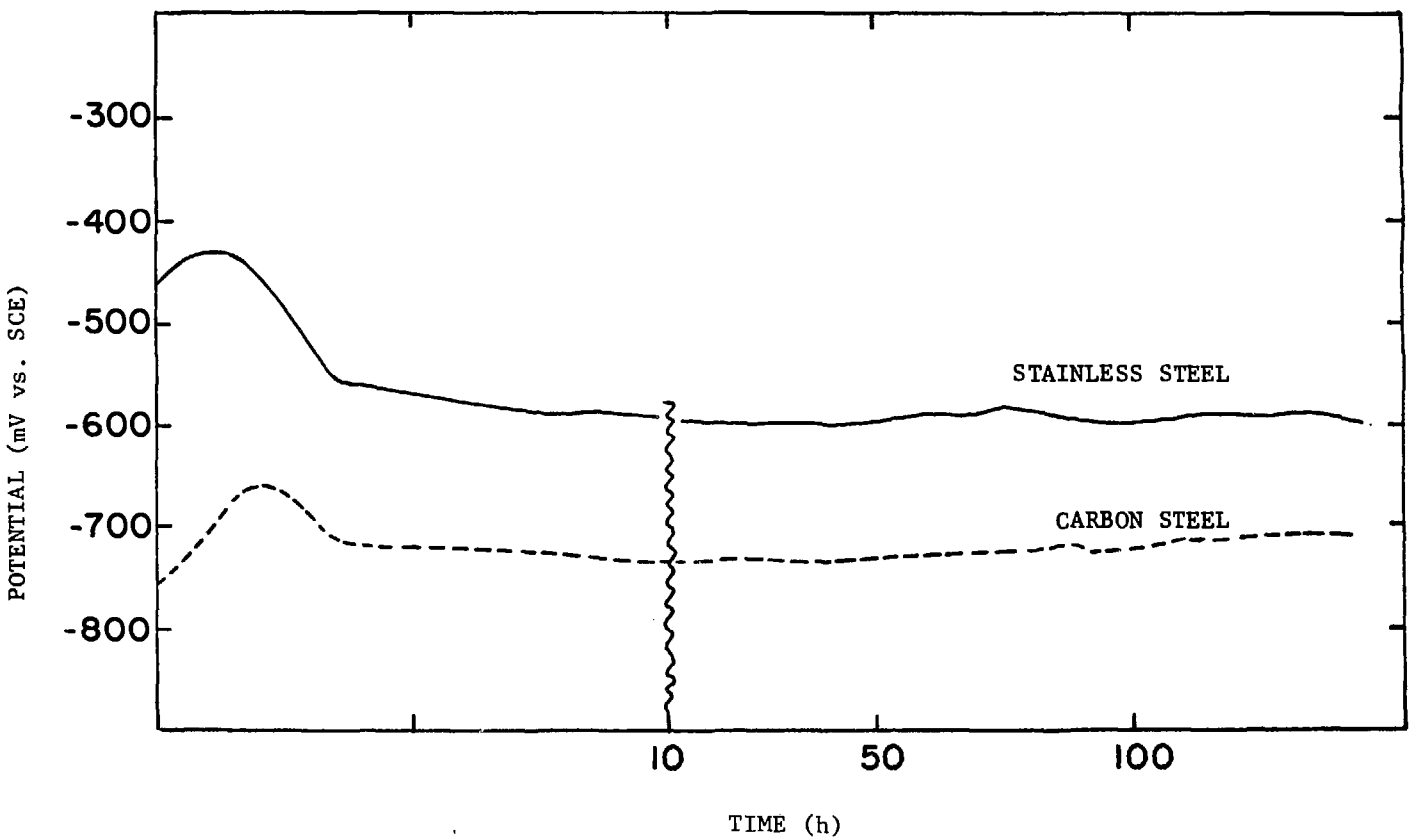


FIGURE 20: Variation of Potential as a Function of Time for Carbon-Steel and Stainless-Steel Electrodes in Aqueous $H_2S$ (Pressure = 1.4 MPa, T = 100°C)

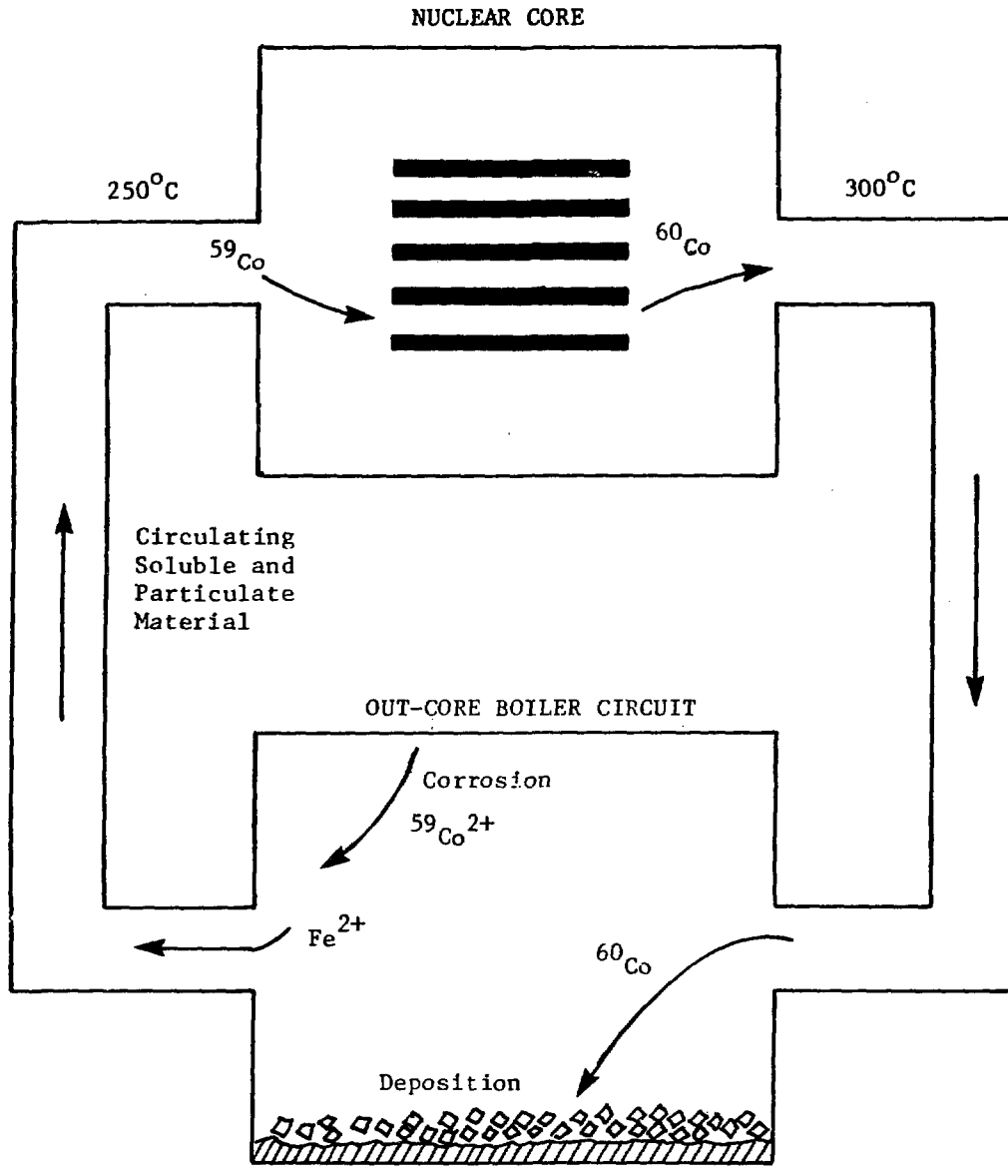


$^{60}Co$ INCORPORATED IN CORROSION FILMS
($Fe_3O_4$; $NiFe_2O_4$; $CoFe_2O_4$)

FIGURE 21: Activity Transport in Nuclear Reactors

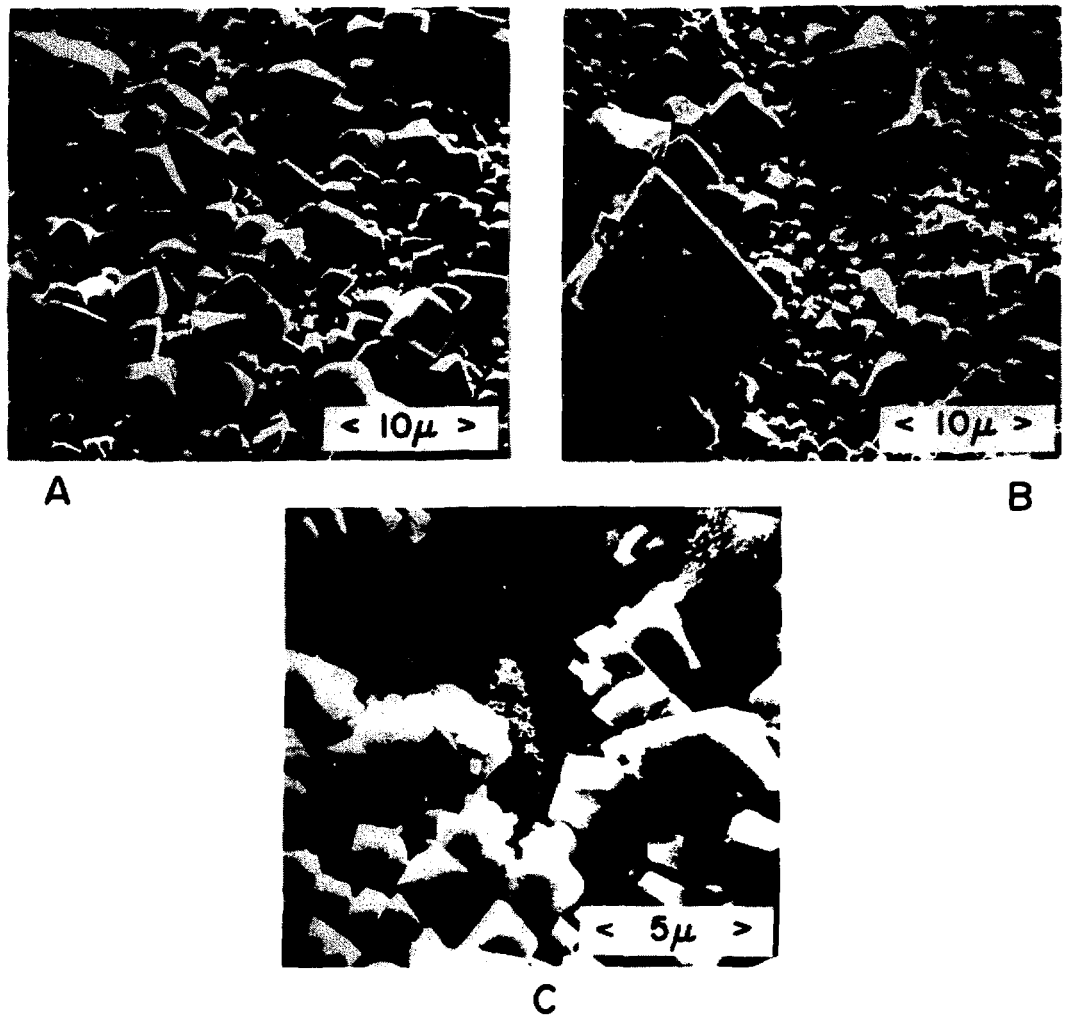


FIGURE 22: Morphology of Magnetite Films Before and After Dissolution in $2 \times 10^{-3}$ mol.dm$^{-3}$ NaEDTA (pH = 3.3, T = 21°C)
(A) Prior to Dissolution; (B) Immediately After Transition from Region II to Region III (See Figure 23); (C) After 6.7 Hours of Dissolution

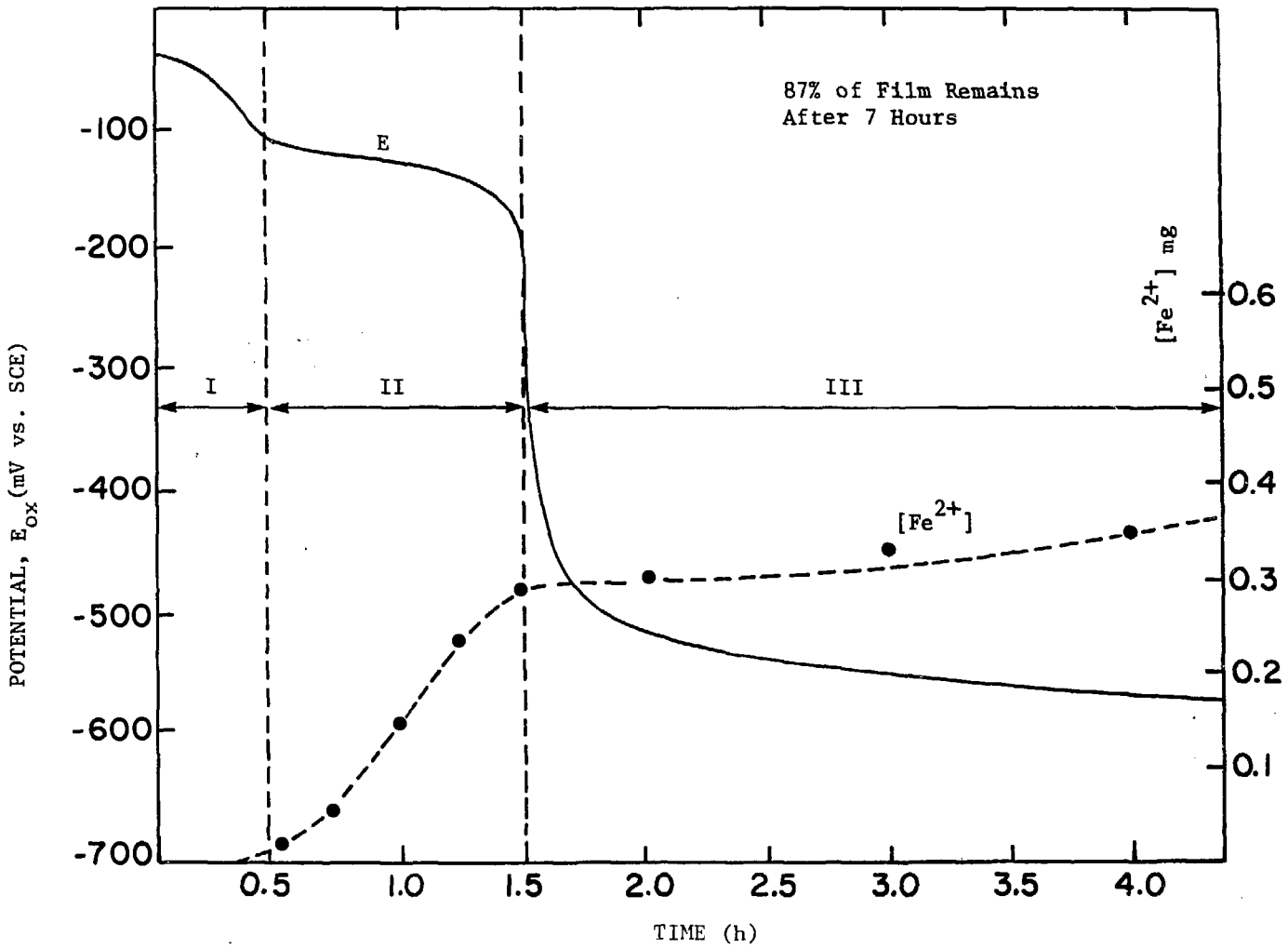


FIGURE 23: Potential Transient ($E_{ox}$) and Total Dissolved $Fe^{2+}$ for the Dissolution of a Magnetite Film in 2 x $10^{-3}$ mol.dm$^{-3}$ NaEDTA; pH = 3.3, T = 21°C.

REGION 1

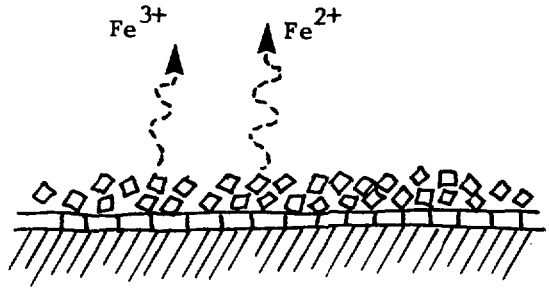


Direct Dissolution

$$Fe_3O_4 + 8H^+ \longrightarrow 2Fe^{3+} + Fe^{2+} + 4H_2O$$

REGION 2

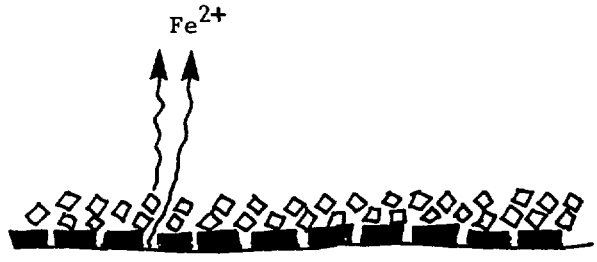


Autoreduction

$$Fe_3O_4 + 8H^+ + 2e \longrightarrow 3Fe^{2+} + 4H_2O$$

$$Fe \longrightarrow Fe^{2+} + 2e$$

REGION 3

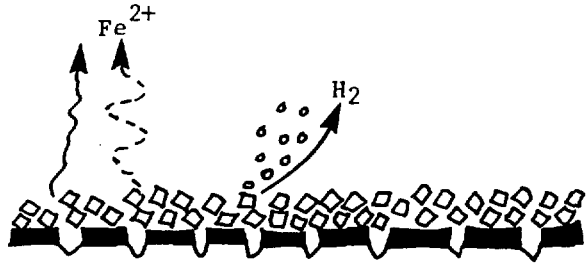


Inefficient Autoreduction

$$Fe_3O_4 + 8H^+ + 2e \longrightarrow 3Fe^{2+} + 4H_2O$$

$$Fe \longrightarrow Fe^{2+} + 2e$$

$$2H^+ + 2e \longrightarrow H_2$$

FIGURE 24: Stages During the Dissolution of Magnetite Films in NaEDTA Solutions

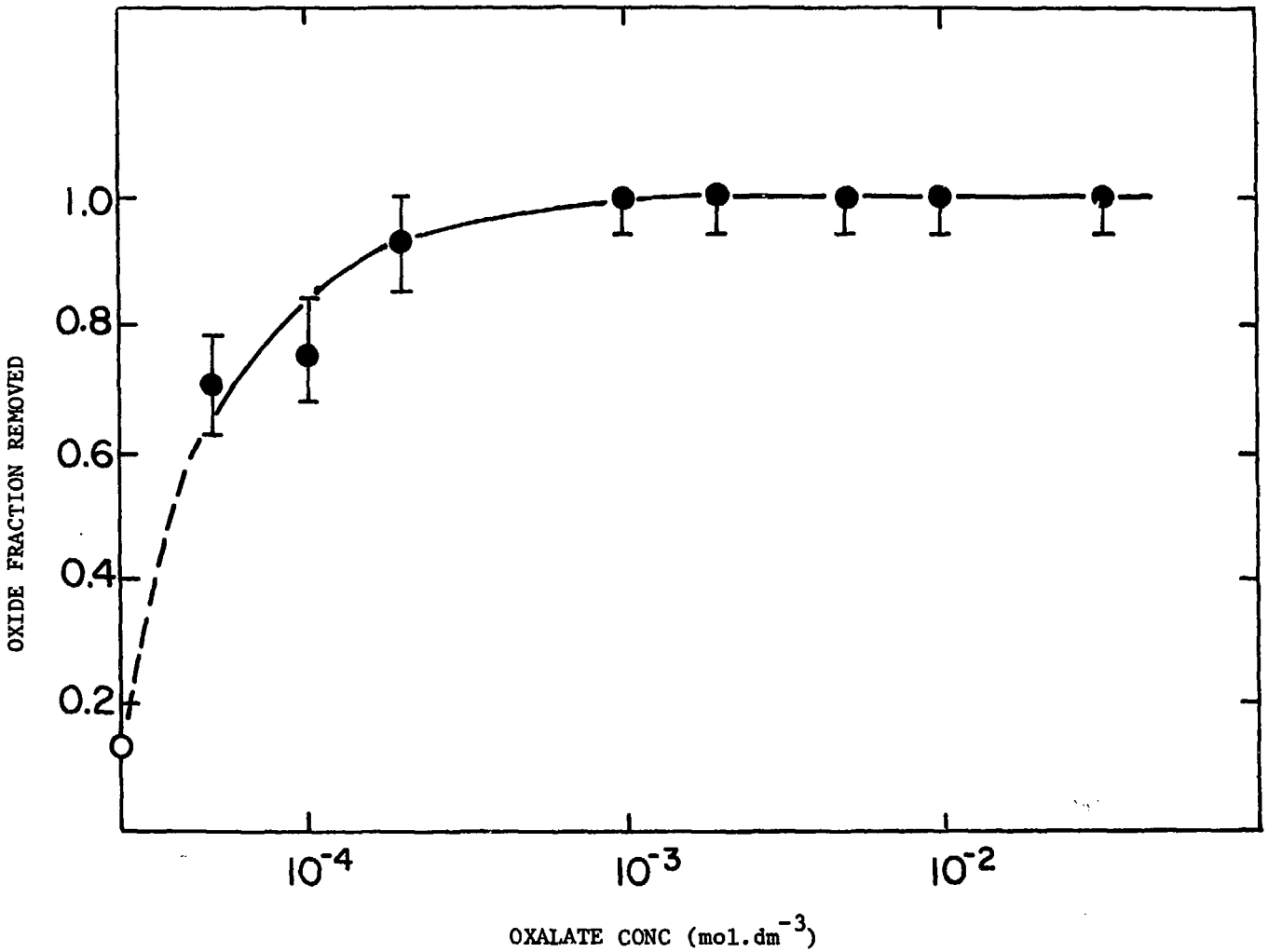


FIGURE 25: Fraction of Oxide Film Removed as a Function of Oxalate Concentration in 2 x $10^{-3}$ mol.dm$^{-3}$ NaEDTA; pH = 3.3; o - Represents the Fraction Removed in the Absence of Oxalic Acid

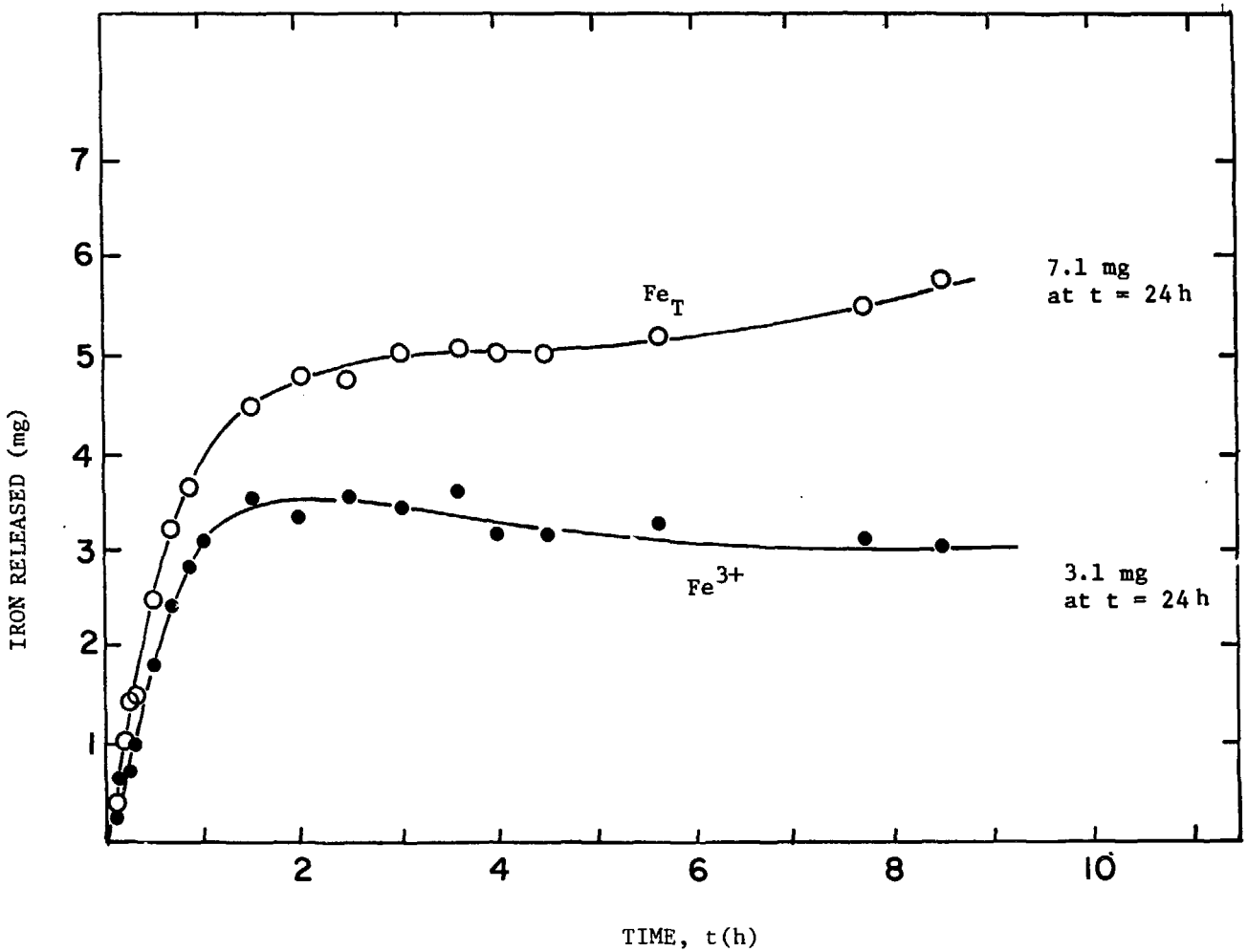


FIGURE 26: Iron Release Profiles for Magnetite Dissolution in $3 \times 10^{-2}$ mol.dm$^{-3}$ Oxalic Acid; pH = 3.3; T = 25°C; $Fe_T$ - Total Iron Released; $Fe^{3+}$ - Ferric Iron Released

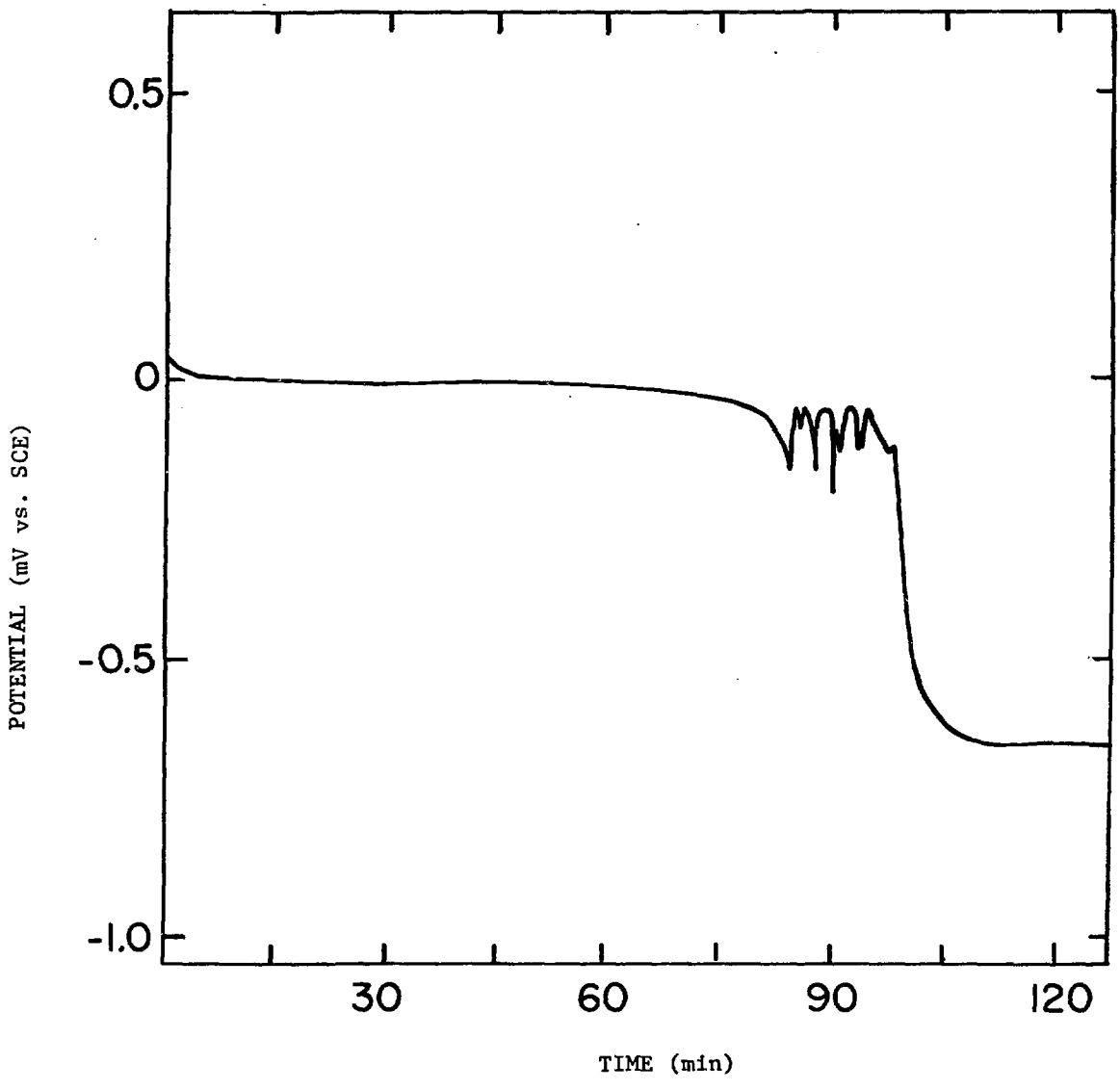


FIGURE 27: Potential Transient for the Dissolution of Magnetite-Covered Iron Discs in 3 x $10^{-2}$ mol.$dm^{-3}$ Oxalic Acid; pH = 3.3; T = 25°C

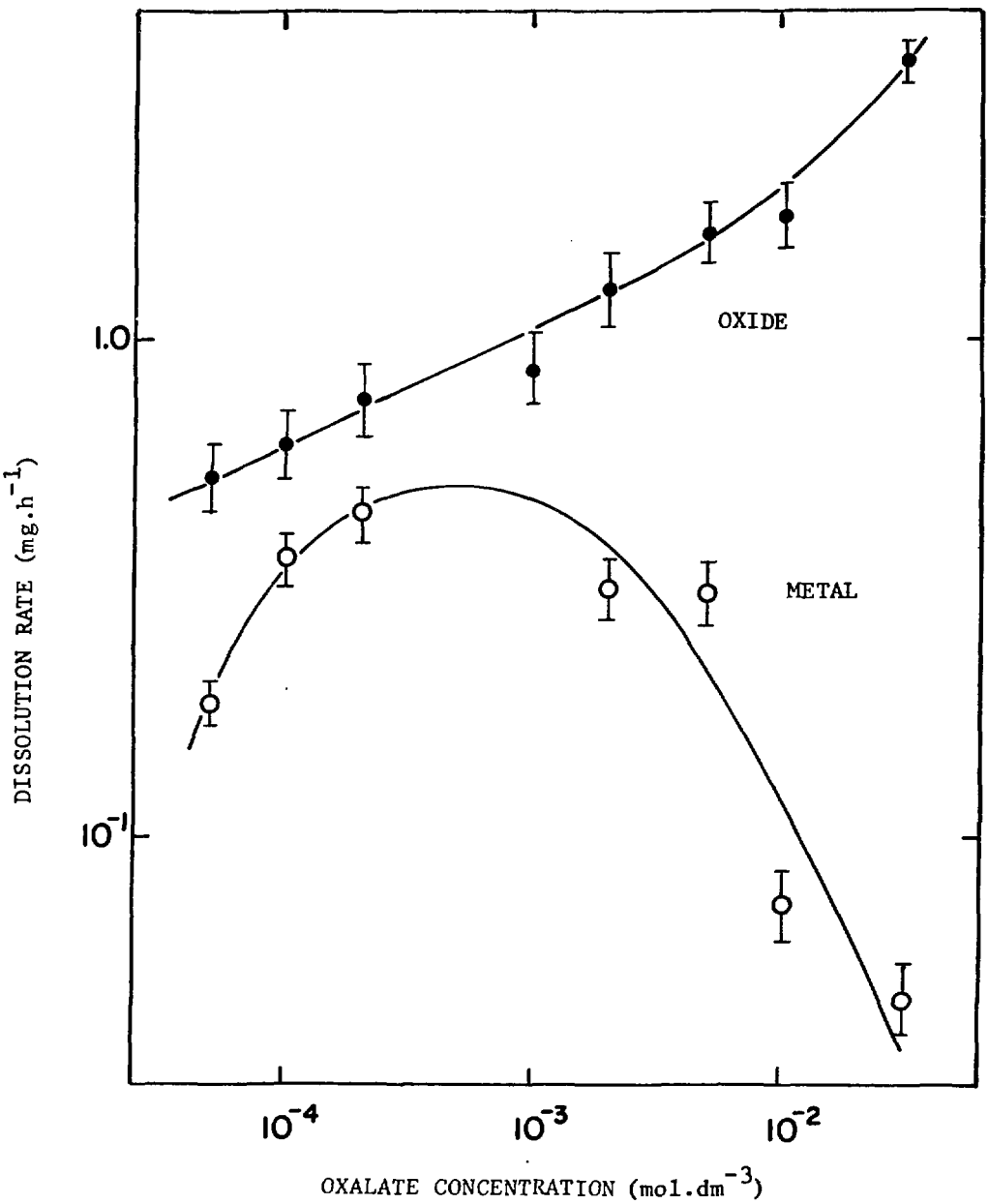


FIGURE 28: Dissolution Rates Calculated from the Slopes of Iron Release Profiles Similar to Those Shown in Figure 26. The oxide dissolution rates were taken from the initial slopes and the metal dissolution rates from the data at times > 4 hours. The base solution contained 2 x $10^{-3}$ mol.dm$^{-3}$ NaEDTA; pH = 3.3, and T = 25°C.

ISSN 0067-0367

To identify individual documents in the series we have assigned an AECL- number to each.

Please refer to the AECL- number when requesting additional copies of this document from

Scientific Document Distribution Office
Atomic Energy of Canada Limited
Chalk River, Ontario, Canada
KOJ 1JO

Price: $5.00 per copy

ISSN 0067-0367

Pour identifier les rapports individuels faisant partie de cette série nous avons assigné un numéro AECL- à chacun.

Veuillez faire mention du numéro AECL -si vous demandez d'autres exemplaires de ce rapport au

Service de Distribution des Documents Officiels
L'Energie Atomique du Canada Limitée
Chalk River, Ontario, Canada
KOJ 1JO

prix: $5.00 par exemplaire